



**Australian Government**  
**Bureau of Meteorology**



# **BARPA-C: Trialling of Convection Permitting Regional Climate Modelling for the Australian Climate Service**

**Emma Howard, Chun-Hsu Su, Christian Stassen, Harvey Ye, Mathew Lipson, Sugata Narsey, Charmaine Franklin**

**June 2025**





# **BARPA-C: Trialling of Convection Permitting Regional Climate Modelling for the Australian Climate Service**

Emma Howard, Chun-Hsu Su, Christian Stassen, Harvey Ye, Mathew Lipson, Sugata Narsey, Charmaine Franklin

Bureau of Meteorology, Australia

Bureau Research Report No. 114

June 2025

National Library of Australia Cataloguing-in-Publication entry

Authors: Emma Howard, Chun-Hsu Su, Christian Stassen, Harvey Ye, Mathew Lipson, Sugata Narsey, Charmaine Franklin

Title: BARPA-C: Trialling of Convection Permitting Regional Climate Modelling for the Australian Climate Service

ISBN: 978-1-925738-57-5

ISSN: 2206-3366

Series: Bureau Research Report – BRR114



Enquiries should be addressed to:

Lead Author: Emma Howard

Bureau of Meteorology  
Level 16, 32 Turbot Street, Brisbane  
Queensland 4000, Australia

[emma.howard@bom.gov.au](mailto:emma.howard@bom.gov.au)

## Copyright and Disclaimer

© Commonwealth of Australia 2025

Published by the Bureau of Meteorology

To the extent permitted by law, all rights are reserved and no part of this publication covered by copyright may be reproduced or copied in any form or by any means except with the written permission of the Bureau of Meteorology.

The Bureau of Meteorology advise that the information contained in this publication comprises general statements based on scientific research. The reader is advised and needs to be aware that such information may be incomplete or unable to be used in any specific situation. No reliance or actions must therefore be made on that information without seeking prior expert professional, scientific and technical advice. To the extent permitted by law and the Bureau of Meteorology (including each of its employees and consultants) excludes all liability to any person for any consequences, including but not limited to all losses, damages, costs, expenses and any other compensation, arising directly or indirectly from using this publication (in part or in whole) and any information or material contained in it.



# Contents

<b>Executive Summary .....</b>	<b>6</b>
<b>1. Introduction .....</b>	<b>7</b>
1.1. Resolution Dependence.....	7
1.2. Hazard Representation in CPMs .....	7
1.3. CPM in Australia .....	8
1.4. Climate Modelling in the ACS .....	9
1.5. BARPA-C Development.....	9
<b>2. Model Configuration.....</b>	<b>10</b>
2.1. Physics and Dynamics .....	11
2.2. Ancillaries.....	11
2.3. Nudging.....	12
<b>3. Performance Assessment of evaluation experiments .....</b>	<b>13</b>
3.1. Mean State Assessment.....	13
3.2. Northern Australian Monsoon .....	17
3.3. Short Duration Rainfall Extremes .....	19
3.4. Tropical Low-Pressure Systems .....	21
<b>4. Trial Assessment.....</b>	<b>23</b>
4.1. Boundary Widths.....	24
4.2. ACCESS-A Land Use Ancillaries .....	25
4.3. Urban Land Surface Modifications.....	28
4.4. Spectral Nudging .....	31
<b>5. Discussion and Conclusions.....</b>	<b>34</b>
5.1. Performance Benchmarks .....	34
5.2. Lessons learned for future trials .....	35
5.3. Limitations and future plans .....	35
<b>Acknowledgements.....</b>	<b>36</b>
<b>References.....</b>	<b>37</b>



## List of Figures

Figure 1: BARPA-C domain (green) over Australia nested in the larger BARPA-R domain (map extent). Australia land area is disaggregated into eight National Resource Management (NRM) spatial clusters, following Clark et al. (2015). ..... 11

Figure 2: Biases in seasonal-mean daily maximum temperatures (tasmax) in BARPA-R, BARPA-C FR and BARPA-C SN, as compared to AGCD. Units are in degrees Celsius. The bottom-left annotation gives the root mean square error averaged over all grid-cells..... 14

Figure 3: Biases in seasonal-mean daily minimum temperatures (tasmin) in BARPA-R, BARPA-C FR and BARPA-C SN, as compared to AGCD. Units are in degrees Celsius. The bottom-left annotation gives the root mean square error averaged over all grid-cells. .... 15

Figure 4: Biases in seasonal-mean precipitation in BARPA-R, BARPA-C FR and BARPA-C SN, as compared to AGCD. Units are in mm/month. The bottom-left annotation gives the root mean square error averaged over all grid-cells. .... 16

Figure 5: DJF-mean 850 hPa winds in ERA5, BARPA-R, BARPA-C\_FR and BARPA-C\_SN. ... 17

Figure 6: Cumulative rainfall averaged over Northern Australia (top) per wet season and (bottom) for the duration of the trail. Rainfall is averaged over the monsoonal north and wet tropics NRM clusters shown in Figure 1. The observational reference is AGCD. .... 18

Figure 7: Biases in December to February-mean precipitation in BARPA-R, BARPA-C\_FR and BARPA-C\_SN, as compared to GPM-IMERG. Units are in mm/month. Note the colour limits are different to Figure 4..... 19

Figure 8: 10-year Annual mean of hourly maximum precipitation rate (RX1H) across BARPA-R, BARPA-C\_FR and BARPA-C\_SN, compared to station data. Top row: full fields of modelled RX1H. Middle row: observed RX1H (left) and RX1H interpolated to station locations using nearest-neighbour regridding. Bottom: bias in RX1H at station locations. . 20

Figure 9: Modelled and observed distribution of hourly rainfall at (a) Gove, (b) Mackay and (d) Sydney Terrey Hills radars. Panel (c) shows a map of radar location, with radar-based RX1H shown in colours. Radar and BARPA-C data have been regridded conservatively to the BARPA-R grid, and only time-steps with valid radar data are considered..... 21

Figure 10: Tropical cyclone track frequencies across BARPA-R, BARPA-C\_FR and BARPA-C\_SN compared to IBTRaCS. Top row: scatterplot of all cyclone locations derived from daily mean data, with minimum pressure indicated by colours. Middle row: heatmap frequency plots of cyclone locations on 4\*4 degree grid. Bottom row: difference of frequency heatmaps between BARPA models and IBTRaCS..... 22

Figure 11: Frequency count of days with tropical low-pressure systems identified, against central pressure. The y-axis is log-scaled. Frequency counts below 955 hPa are annotated on the figure. .... 23

Figure 12: Boundary effects on key variables by latitude..... 25

Figure 13: Fraction of each grid-cell undergoing land use type transformation for each major land use transformation pair as per text. The final panel provides a key for the NRM spatial clusters. .... 26



Figure 14: NRM Cluster-mean change in diurnal temperature range, (top row) tasmax (middle row) and tasmin (bottom row) in the region of each land use type transform pair (as per text) between trial\_LU\_CCI and trial\_LU\_AA. .... 27

Figure 15: Timeseries of NRM cluster mean soil moisture in regions where the land-use type is updated (as per Figure 2). Soil moisture is summed across the top two soil model layers and has units of kg/m3. Only cluster/land use transformation pair combinations with a substantial change in soil moisture are shown. trial\_LU\_AA is shown in blue, while trial\_LU\_CCI is shown in orange. .... 28

Figure 16: Time series of urban soil moisture in Sydney in BARPA-R and in the urban and land-use trials. Orange: average across region with urban tile fraction >0.5. Blue: average across bushland adjacent to Sydney (urban tile fraction <0.2). .... 30

Figure 17: DJF-mean 850 hPa winds as per figure 5 but for the spectral nudging trials. .... 32

Figure 18: RX1D bias against AGCD. All datasets were regridded to the BARPA-R grid before index calculation. .... 33

Figure 19: Tropical cyclone intensities as per figure 11 for spectral nudging trials. .... 33

**List of Tables**

Table 1: Targeted Trial descriptions. .... 23

Table 2: Spectral nudging parameters across regional modelling studies. Where a length-scale was recommended by the study, it is indicated in bold. .... 31



## Executive Summary

Convection permitting climate modelling and projections have the potential to provide reliable climate change information at regional and local scales that are relevant for informing climate adaptation decisions. The Bureau of Meteorology is developing the capability to extend regional-scale climate projections to convection-permitting scales using the BARPA (Bureau of Meteorology Atmospheric Regional Projections for Australia) framework. This paper documents the development process for the first convective-scale BARPA (BARPA-C) configuration used to generate research-focussed time-slice projections over Australia for the first phase of Australian Climate Service (ACS). It describes the model configuration, performance at simulating mean and extreme climates, and the trials used to make key decisions about configuration choices. BARPA-C is shown to provide a step-change improvement in the representation of climate extremes such as short-duration high intensity rainfall and intense tropical cyclones. However, key model biases including a dry bias in northern Australia, persist and will be targeted by future development.



# 1. Introduction

Convection-permitting atmospheric models (CPMs) have been used by the Bureau of Meteorology to generate short-term weather forecasts since 2017. By explicitly simulating convection and hence removing propagating errors that originate in convection schemes, CPMs are widely regarded to produce substantially more skilful forecasts of weather hazards than coarser resolution convection parametrised models. They achieve this improved skill by simulating more accurate representations of the processes and characteristics of weather events. One prominent example is the ability of CPM forecasts to produce more accurate rain-rate distributions and spatiotemporal characteristics of extreme rainfall (Fosser et al., 2015).

## 1.1. Resolution Dependence

CPMs can represent a step-change improvement in the simulation of precipitation because of the resolution of length-scales at which storm-scale processes may start to be explicitly simulated, rather than parameterised (Clark et al., 2016). However, these storm-scale processes occur across a spectrum of length-scales, and horizontal grid-spacings around 100m are required before a model resolves finer scale storm processes (Bryan et al., 2003; Lean et al., 2024). Benefits to the representation of rainfall climates have been found to level off at a 'sweet spot' around 1km in current model simulations (Potvin & Flora, 2015; Stein et al., 2015). Generally, however, the benefits of explicitly simulating convection are much greater than those gained by simply increasing the grid-spacing above 4km (Holloway et al., 2013; Vergara-Temprado et al., 2020). Typically, CPM projection grid-spacings vary between 2 and 4 km (Lucas-Picher et al., 2021), with 4 km generally accepted to be coarsest grid-spacing where convection parameterisation schemes are not required (Weisman et al., 1997). However, most CPM climate simulations on domains that are larger than 4000×4000 km<sup>2</sup> tend to use resolutions at the coarser end of this range. Continental-scale CPM-based climate projections using a 4-km grid-spacing have been generated across the world, including in North America (Liu 2017), South America (Liu et al., 2025), and Africa (Senior et al., 2021; Stratton et al., 2018).

## 1.2. Hazard Representation in CPMs

While CPMs are accepted as the norm in weather forecasting, their uptake by the climate modelling community has been more gradual, mostly due to the very high computational expense of testing and running CPM simulations for longer climate timescales. However, the same improvements in forecasted weather events allow convection-permitting climate projections to simulate the frequencies and intensities of many hazardous weather systems more accurately and to project these hazard characteristics into the future. Hence, CPMs have the potential to provide a substantial improvement to the risk assessment of natural hazards into the future.

Weather hazards associated with short duration high intensity convective rainfall are particularly sensitive to the representation of atmospheric convection in climate models.



The nature of atmospheric convection depends strongly on atmospheric temperature and humidity profiles, which are projected to be affected by climate change. Studies of contemporary climate change have reported increases in the frequency of the most intense rainfall rates across the world and across length scales (Bao et al., 2017; Donat et al., 2017; Wasko et al., 2024). These heavy rain-rates are poorly represented in convection parameterised models, and CPMs have been shown to be more capable of simulating projections of increased heavy rainfall (Kendon et al., 2023). CPMs typically show stronger intensification of extreme rainfall than their convection-parametrised Regional Climate Model (RCM) counterparts (Lee et al., 2022; Luu et al., 2022), as well as a reduction in the spread and associated uncertainty in extreme rainfall projections (Fosser et al 2020). Additionally, convective weather systems such as tropical cyclones have been shown to be better represented in CPM simulations compared to traditional RCM simulations (Buonomo et al., 2024).

The improved representation of precipitation can have flow-on effects to other hazards such as flash flooding. Driving hydrological models using bias-corrected inputs derived from CPM has been demonstrated to add value in the simulation of historical climatologies of flood peaks (Poncet et al., 2024). They found that in the Mediterranean, CPM-based projections diverged from traditional RCM-based projections, with the most extreme floods becoming more intense, but more moderate floods becoming less frequent.

As well as the representation of convection, other improvements derive from a decreased grid-spacing, namely the representation of coastlines, topography, and urban areas (Cortés-Hernández et al., 2024; Langendijk et al., 2021)(Cortés-Hernández et al., 2024; Kruk et al., 2010). Improved simulation of urban centres, where exposure to extreme weather events is high, is crucial for climate risk assessment. Another critical effect of convection permitting resolutions is an expected improvement of the simulation of mesoscale features, such as mesoscale convective systems, frontal rainbands and wind shift lines, sea-breezes, orographic circulations and the larger scale weather systems they are embedded in (Belušić Vozila et al., 2024; Cortés-Hernández et al., 2024; Maybee et al., 2024). These improvements have direct relevance for hazard simulation. For example, bushfires behaviour in southern Australia is significantly impacted by passing weather fronts. The structure of the front's wind field, which can often cause a sudden change in the direction of bushfire spread, is sensitive to the explicit representation of convection (Dowdy et al., 2021).

### 1.3. CPM in Australia

In Australia, CPMs have been used to produce climate projections for regional domains, however, to date no unified Australia-wide CPM simulations are available. The Energy Sector Climate Information project (CSIRO and Bureau of Meteorology, 2021) presented two prototype BARPA-C configurations, based on CMIP5, providing projections over two subregions of eastern Australia, a northern and a southern domain. Brown et al., (2024) demonstrated that the representation of wind gusts in the southern domain were significantly improved over the convection-parametrised counterpart. More recently, the



NARCLIM2.0 projections based on CMIP6 include a convection-permitting component covering southeastern Australia (Di Virgilio et al., 2024).

## 1.4. Climate Modelling in the ACS

The Australian Climate Service (ACS) is investigating the value-add that CPMs provide to climate hazard projections through generation and analysis of a targeted set of downscaled climate projections utilising a 4-km grid-spacing. The Bureau of Meteorology will contribute to this exercise by producing dynamically downscaled projections using the BARPA-C (Bureau Atmospheric Regional Projections for Australia: Convective) limited area climate model, which is an ACCESS-based, convection permitting atmosphere-land system model. ACCESS (Australian Community and Earth-System Simulator) is the local implementation of UK Met Office Unified Model (MetUM) for the atmosphere and Joint UK Land Environment Simulator (JULES) for the land surface.

BARPA-C builds upon its regional counterpart, BARPA-R, which downscaled 7 general circulation models over an Australasian domain to a 17-km grid-spacing using a convection-parametrised MetUM configuration. BARPA-R configuration details are provided by Su et al., (2022), with evaluation performed by Howard et al., (2024), Jiang et al., (2025) and Stassen et al., (2025). BARPA-R has been shown to well simulate the temperature and precipitation climate over Australia and has been used to inform the National Climate Risk Assessment (Jakob et al., 2025).

The ACS favours a multi-model ensemble-based approach for downscaling climate projections, using a sparse matrix of multiple GCMs, RCMs and CPMs. As such, all BARPA-based modelling is complemented by experiments using the Conformal-Cubic Atmospheric Model (CCAM). (Schroeter et al., 2024) documents the performance of the regional-scale CCAM experiments, while convective-scale CCAM is currently under development.

## 1.5. BARPA-C Development

To select the BARPA-C configuration used for the initial ACS phase 1 prototype BARPA-C projections, a series of trials and evaluation experiments were run. First, a set of targeted trials were run to determine an initial model configuration. Trial lengths ranged from several months to a year. Targeted trials estimated the width of boundary edge effects in the output data, tested new land surface ancillaries and trialled options for urban soil moisture. This configuration was used to run the first ERA5 evaluation experiment, labelled BARPA-C\_FR throughout this paper.

The BARPA-C\_FR experiment used a free-running set-up, with prognostic variables evolving freely away from the lateral boundaries. Following assessment against observations, this experiment was found to poorly simulate the northern Australian monsoon, with weak monsoon westerlies, reduced tropical cyclone frequencies and a reduction in the mean-state precipitation in Northern and interior Australia during the wet season.



To address the dry bias in BARPA-C\_FR, additional trials were run to test the introduction of spectral nudging with the goal of maintaining the monsoon circulation, which was well simulated by BARPA-R. Spectral nudging is a downscaling technique that relaxes the large-scale circulation to match the driving model, while allowing small-scales to evolve freely. A revised evaluation experiment, labelled BARPA-C\_SN, was then conducted using the selected spectral nudging configuration.

This paper documents the BARPA-C modelling configuration, evaluation experiment assessment and trial results. First in section 2, the model configurations used in the two evaluation experiments are presented. These configurations are identical with the exception of the spectral nudging in the second experiment. Second, the ability of both evaluation experiments to represent the mean state and hazard-relevant climate extremes is assessed in section 3. This section includes an assessment of the northern Australian monsoon circulation, and its improvement in the spectral nudging experiment. Third, the trials used to set up the model configurations, including the spectral nudging trials, are documented in section 4. Limitations, the path forward and lessons learned are discussed in section 5.

## 2. Model Configuration

BARPA-C uses MetUM (Davies et al., 2005), coupled to JULES (Best et al., 2011). The MetUM has a non-hydrostatic, fully compressible, deep atmosphere formulation. It solves a formulation of the equations of motion using a semi-implicit iterative method, solving for prognostic variables 3D winds, virtual dry potential temperature, Exner pressure, dry density, hydrometeor mixing ratios, and hydrometeor number concentrations for rain, snow, graupel and ice. Spatial discretisation uses a regular Plate Carree projection and a staggered Arakawa C grid in the horizontal and a vertically staggered, stretched hybrid height Charney-Phillips grid in the vertical (Charney & Phillips, 1953). The horizontal grid has a constant grid-spacing 0.04 degree in the zonal and meridional dimensions, roughly equivalent to 4.4 km at the equator. The vertical grid has 70 levels, has a 40-km model top, and the first model level is 2.5m above ground level away from topography. Sea surface temperature is prescribed as a lower boundary condition and is derived from the driving global model.

The JULES land-surface scheme models 10 land-use categories and four soil levels. The land-use categories consist of 5 plant functional types (broadleaf trees, needleleaf trees, temperate C3 grass, tropical C4 grass, and shrubs) and 5 non-vegetated types (inland water, bare soil, land ice, urban roof and urban canyon). The latter 2 categories are used in the MORUSES urban scheme (Porson et al., 2010). The soil layers have respective thicknesses 0.1, 0.25, 0.65 and 2.0 metres, with a total depth of 3 metres.

BARPA-C is a limited area model, with lateral boundaries at 107E, 161E, -46.7S and -4 S. All trials described in this document are nested within BARPA-R-ERA5, described in Su et al 2022 and evaluated by Howard et al., (2024). BARPA-R-ERA5 is considered an evaluation experiment where the regional model is nested in ERA5 (Hersbach et al., 2020, 2018a, 2018b) that is assumed to be relatively unbiased as compared to a global



climate simulation experiment. Domain boundaries of BARPA-C are shown in Figure 1 and were determined using trials described in section 4.1 below.

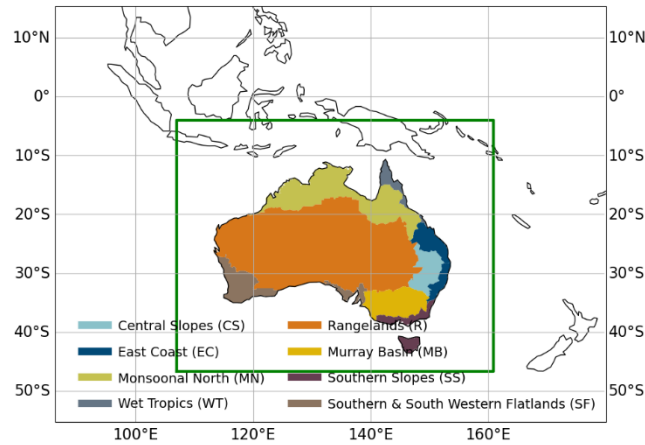


Figure 1: BARPA-C domain (green) over Australia nested in the larger BARPA-R domain (map extent). Australia land area is disaggregated into eight National Resource Management (NRM) spatial clusters, following Clark et al. (2015).

## 2.1. Physics and Dynamics

BARPA-C uses the Regional Atmosphere and Land science configuration version 3.2 (RAL3.2, Bush et al., 2024). RAL3.2 features only explicit, unparametrized convection, and uses an implementation of the CASIM microphysics scheme (Field et al., 2023) to model five hydrometeor species: cloud droplets, rain, ice, snow and graupel. This implementation models two moments for rain, ice, snow and graupel, and one moment for cloud droplets, whose number concentrations are prescribed. The dynamical core (ENDGame) is semi-implicit, semi-Lagrangian and solves the non-hydrostatic, fully compressible equations of motion (Wood et al., 2014). Other parameterisations include the SOCRATES radiative transfer scheme (Edwards & Slingo, 1996; Manners et al., 2024), a new bimodal cloud scheme (Van Weverberg, 2021a,b), and the blended boundary layer scheme described by Boutle et al., (2014). This boundary layer scheme blends the 1D non-local (Lock et al., 2000) and 3D Smagorinsky, (1963) schemes.

Observed historical aerosol, green-house gas and ozone forcing has been implemented following Tucker et al., (2022). This approach prescribes 4D aerosol optical properties on 9 shortwave and 6 longwave bands in the SOCRATES radiative transfer code, combining seasonal and spatial variation derived from an offline simulation using the Global Model of Aerosol Processes (GLOMAP) scheme (Mann et al., 2010) with interannual variation derived from the EasyAerosol project (Stevens et al., 2017).

## 2.2. Ancillaries

BARPA-C has been co-developed with two other applications of the RAL3.2 configuration: the ACCESS-A weather forecast model (Rennie et al., 2025) and the BARRA-C2 reanalysis (Su et al., 2024). BARPA-C has benefitted from this collaboration



by using land use type ancillaries developed specifically for ACCESS-A. Compared to the UM default land use field (sourced from ESACCI Land Cover v1; Hartley et al., 2017), the changes applied are: sourcing land cover types from CC1v2 (Harper et al., 2023) for natural areas and from WorldCover for urban areas (Zanaga et al., 2021), using the 250m CSIRO Gramina Australian C4 grass fraction dataset for C3/C4 grass partitioning (Donohue, 2023), and modifying the land-sea mask so that all coastal land-based Automatic Weather Station (AWS) sites on the Australian mainland are located on land points. The urban morphology was derived following Bohnenstengel et al., (2011), using empirical relations derived for London. The orographic height ancillary has been sourced from the Global Land One-kilometer Base Elevation (GLOBE) Digital Elevation Model (Hastings et al., 1999). All other ancillaries are standard for RAL3.2, as documented by Bush et al., (2024).

### 2.3. Nudging

Spectral nudging is a technique used in earth system modelling which constrains large-scale atmospheric motion with a prescribed input dataset while allowing small scale motion to evolve independently. As will be discussed in section 3, spectral nudging is used in BARPA-C to rectify a bias in the tropical circulation. Spectral nudging is implemented using a convolution-based method adapted from Uhe & Thatcher, (2015). 3D temperature and horizontal wind prognostic variables are nudged towards the driving model (BARPA-R) at length-scales greater than a synoptic-scale cut off. We follow Uhe & Thatcher, (2015) in only nudging potential temperature and horizontal winds, allowing moist processes to evolve freely. Nudging is achieved through including the following relaxation term into the update equations for potential temperature ( $\theta$ ), and horizontal wind components U and V:

$$\phi'(t_n) = \phi(t_n) - \frac{\Delta t}{e} (\Delta\phi(t_n) * w(L)) \quad (1)$$

Where  $\phi$  is a state variable within a nested model grid to be nudged,  $\Delta\phi$  is the difference between nested model and driving data,  $\Delta t$  is the model integration time step,  $t_n$  denotes the valid time when the nudging increments will be applied,  $e$  is an e-folding time that controls the nudging strength, and  $w$  is the gaussian weighting function with standard deviation given by  $L$ . The Gaussian weighting function is approximated as the product of two orthogonal 1D filters in the meridional and zonal directions.

In our nudged experiment labelled as BARPA-C\_SN, spectral nudging is applied between model levels 21 and 67, which corresponds to approximately 1500m – 30000m above surface, or 850 hPa to 10 hPa. A soft e-folding time of 12-hours was applied, and nudging was only applied to length-scales exceeding 1200 km. These parameters were selected based on trials discussed in section 4.4, which also compares the selected nudging parameters to other modelling experiments.



### 3. Performance Assessment of evaluation experiments

Two evaluation experiments have been conducted, with and without spectral nudging applied. The experiments were 10-years long, with a 3-month spin up period. The simulated spin-up period was September 2012 – November 2012, and the run period was 1/December 2012 – 30/November 2022. Boundary conditions, and the nudging reference where relevant, were sourced from the BARPA-R evaluation experiment.

This section assesses the representation of the mean-state rainfall and temperatures, northern Australian monsoon, extreme rainfall and tropical cyclones in both evaluation experiments. Australian Gridded Climate Data (AGCD version 1) (Jones et al., 2009) is used as the reference dataset for land-based mean temperatures and precipitation, while GPM-IMERG (Huffman et al., 2018) is used to assess rainfall over oceans. ERA5 reanalysis is used as a reference when assessing monsoon winds. Extreme rainfall and winds are compared against AWS data, while tropical cyclones are assessed against the international best track dataset IBTRaCS (Knapp et al., 2010).

The driving model (BARPA-R) is provided as a benchmark for the assessment of BARPA-C's climate. *A priori*, we expect that:

**Benchmark 1:** BARPA-C should not significantly degrade the mean-state compared to BARPA-R, and

**Benchmark 2:** The representation of climate extremes that are intrinsically linked to convective processes is substantially improved in BARPA-C compared to BARPA-R.

#### 3.1. Mean State Assessment

The seasonal mean bias compared with AGCD of daily minimum screen-level temperatures (tasmin), daily maximum screen-level temperatures (tasmax) and rainfall are shown in Figures 2, 3 and 4 respectively for BARPA-R, BARPA-C\_FR and BARPA-C\_SN. All fields are regridded to the coarsest model grid (BARPA-R) using conservative remapping before analysis is commenced. Patterns and values of tasmax biases are extremely similar across all three models, suggesting that the tasmax biases are not affected by the explicit representation of convection, the spectral nudging or any of the other configuration changes introduced in RAL3.2 compared to GA7. Thus, BARPA-C retains the 1-2 degree Celsius winter cold bias in tasmax described by Howard et al., (2024).

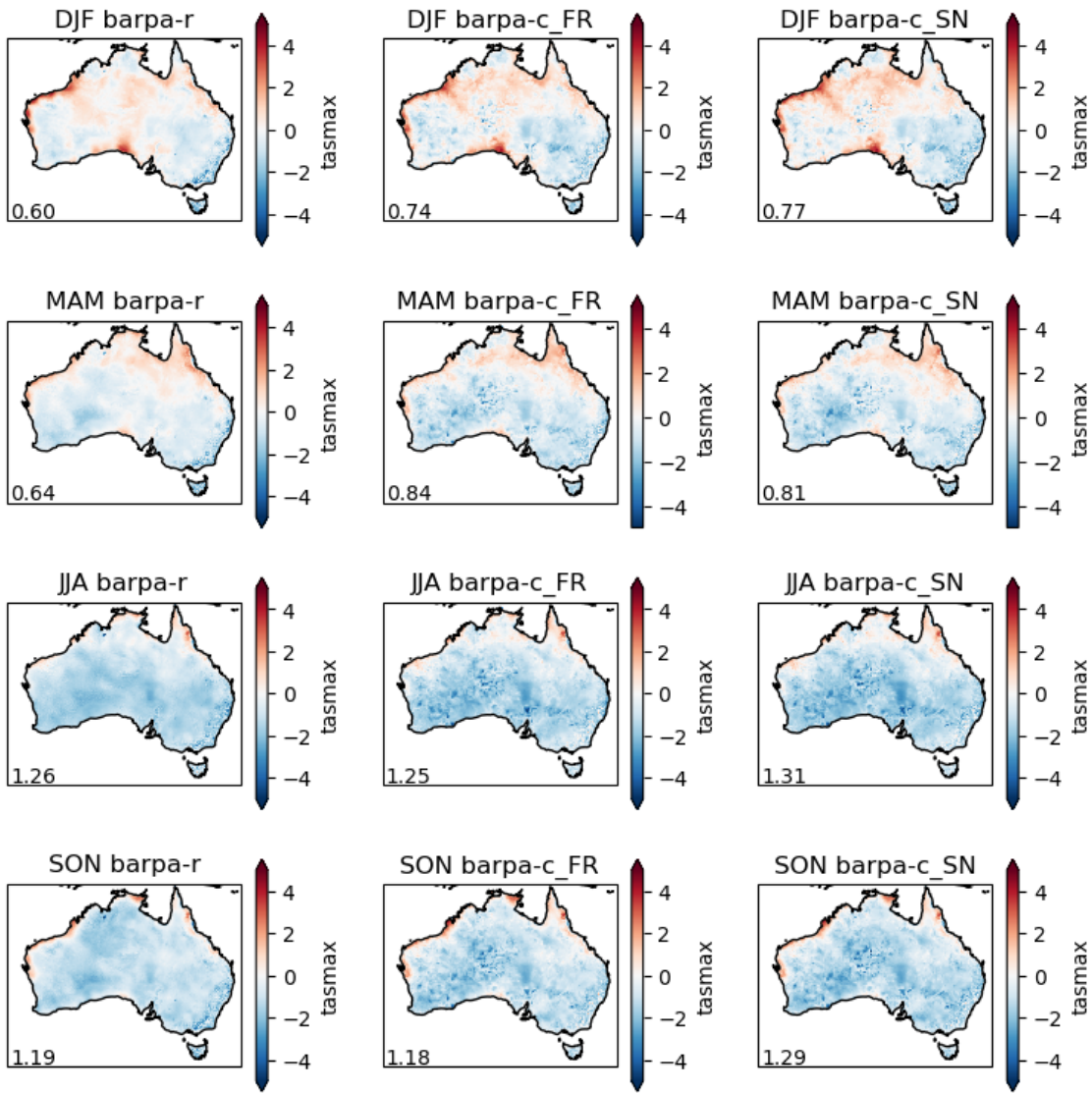


Figure 2: Biases in seasonal-mean daily maximum temperatures (tasmax) in BARPA-R, BARPA-C FR and BARPA-C SN, as compared to AGCD. Units are in degrees Celsius. The bottom-left annotation gives the root mean square error averaged over all grid-cells.

More differences are present between BARPA-R and both BARPA-C experiments when considering overnight tasmin. BARPA-C\_FR and BARPA-C\_SN are still very similar, suggesting that the spectral nudging does not impact tasmin biases. The BARPA-C experiments both show an increased cold bias in summer over much of interior Australia and a reduced warm bias during winter. Overall, therefore, the representation of mean-state tasmin and tasmax in BARPA-C is generally of a similar level of performance as was observed in BARPA-R, meeting benchmark 1.

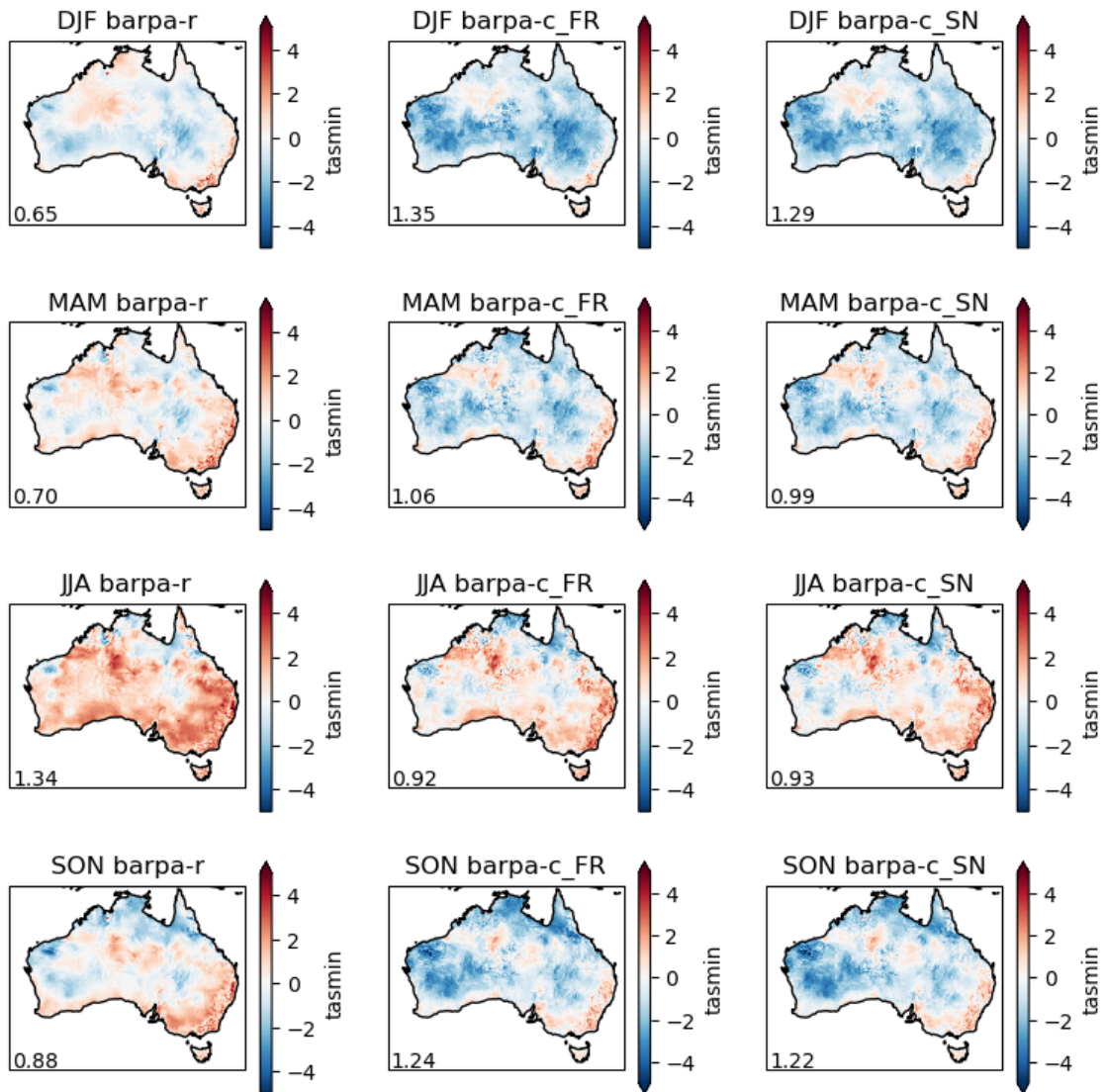


Figure 3: Biases in seasonal-mean daily minimum temperatures (tasmin) in BARPA-R, BARPA-C FR and BARPA-C SN, as compared to AGCD. Units are in degrees Celsius. The bottom-left annotation gives the root mean square error averaged over all grid-cells.

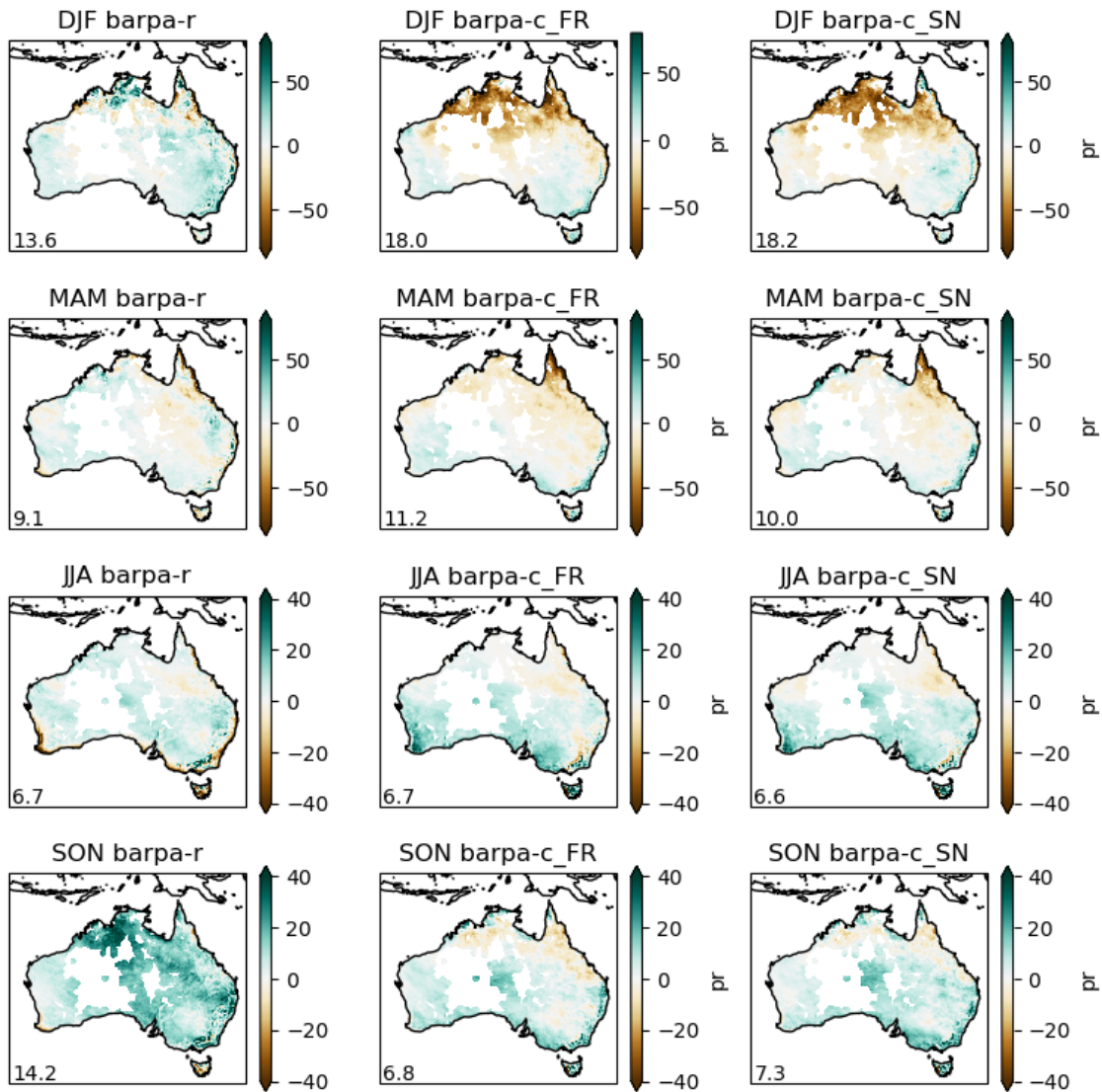


Figure 4: Biases in seasonal-mean precipitation in BARPA-R, BARPA-C FR and BARPA-C SN, as compared to AGCD. Units are in mm/month. The bottom-left annotation gives the root mean square error averaged over all grid-cells.

Figure 4, which shows precipitation biases, raises more issues around the mean-state representation in BARPA-C. Most prominently, BARPA-C\_FR shows reduced rainfall across Northern Australia from December to February, the core of the Austral monsoon. Although the spectral nudging was introduced to improve this monsoon rainfall, BARPA-C\_SN shows a very similar dry bias in Northern Australia over land.

Some improvements in mean-state rainfall are present. In southern Australia on the east and west coasts, winter dry biases are resolved in both BARPA-C experiments, suggesting that the sharp gradients in coastal rainfall are well resolved. Though geographically small, these high-rainfall coastal areas have outsized importance due to the location of cities and population centres. Additionally, the BARPA-R spring wet bias is resolved in BARPA-C.

Overall, mean-state precipitation is well represented in BARPA-C across all regions and seasons except for Northern Australia during the Austral monsoon. The next section examines the monsoon dry bias and associated circulation biases in detail.

### 3.2. Northern Australian Monsoon

Following the discovery of the BARPA-C\_FR northern Australian dry bias, detailed attention was paid to the representation of the Australian Monsoon. The monsoon circulation over northern Australia was found to be shifted north in BARPA-C\_FR, resulting in a decrease in the frequency of the monsoon westerly winds over northern Australia. Due to the close coupling between the monsoon circulation and northern Australian precipitation (Sekizawa et al., 2023), it was unclear whether the dry bias was causing a weakening of the monsoon, or whether the northward shift in the monsoon winds was causing less rainfall over the Australian region. Spectral nudging, described in sections 2.3 and 4.4, was introduced to test the latter hypothesis.

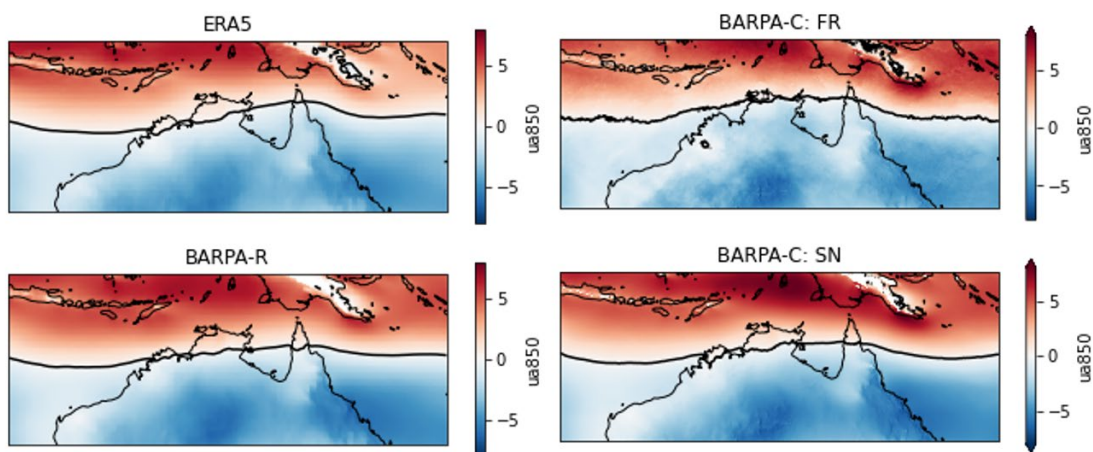


Figure 5: DJF-mean 850 hPa winds in ERA5, BARPA-R, BARPA-C\_FR and BARPA-C\_SN.

Figure 5 shows the mean-state December – March wind zonal winds over northern Australia at 850 hPa in ERA5 and the three BARPA models, with the mean position of the monsoon shearline (the zero-contour of the 850 hPa zonal wind) shown in black. From this plot, it is evident that the monsoon westerly winds are shifted north in BARPA-C\_FR over the Top End, while both BARPA-R and BARPA-C\_SN show monsoon winds that are closer to the reference reanalysis. Over Cape York, BARPA-C\_FR is in fact closer to observations, while both BARPA-R and BARPA-C\_SN show a southward shift in the shearline location. As indicated by Figure 6, this rectified the dry-bias over land for the first four years of the simulation, after which the dry-bias re-emerges.

Figure 6 also highlights the difficulties with assessing short trials nested within BARPA-R. The interannual variability of northern Australian rainfall and the monsoon westerly winds in BARPA-R is decoupled from the driving ERA5 dataset (Howard et al., 2024). Consequently, biases in these fields take a large amount of time to emerge. For example,



the rainfall bias of BARPA-C after the first season appeared to be much improved on BARPA-R, because the 2012-13 season was abnormally wet in BARPA-R, but dry in observations. In subsequent seasons, the BARPA-R wet bias is lessened, and the BARPA-C dry bias begins to become more apparent.

Figure 7 recreates the DJF precipitation biases shown in Figure 4 but uses satellite-based GPM-IMERG as a reference, rather than AGCD. As GPM-IMERG is available over oceans as well as land, a land-mask has not been applied. This reveals that the dry bias is significant over the seas north of Australia in BARPA-C\_FR but rectified there in BARPA-C\_SN. This analysis indicates that the dry bias over land is not caused by the shift in the monsoon winds. However, spectral nudging has been able to improve the large-scale circulation, which may have flow-on effects for the representation of hazardous weather in the tropics.

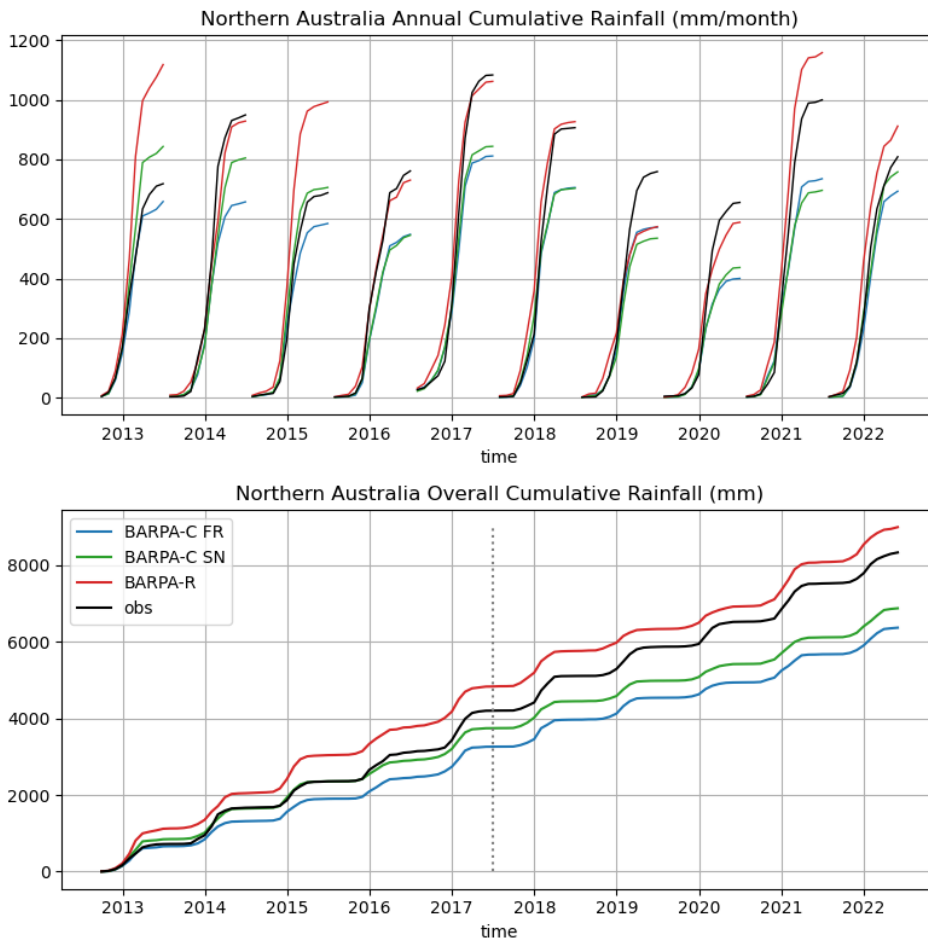


Figure 6: Cumulative rainfall averaged over Northern Australia (top) per wet season and (bottom) for the duration of the trail. Rainfall is averaged over the monsoonal north and wet tropics NRM clusters shown in Figure 1. The observational reference is AGCD.

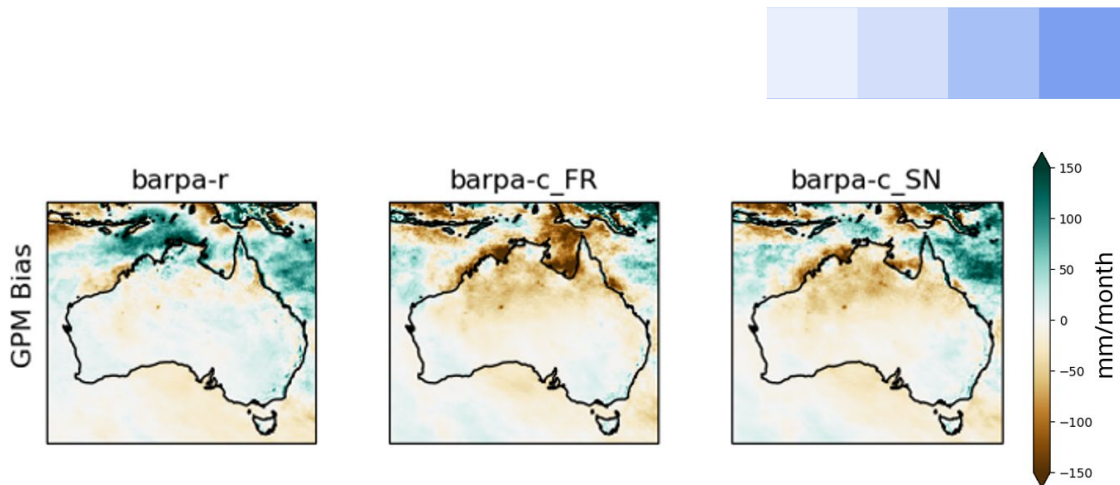


Figure 7: Biases in December to February-mean precipitation in BARPA-R, BARPA-C\_FR and BARPA-C\_SN, as compared to GPM-IMERG. Units are in mm/month. Note the colour limits are different to Figure 4.

### 3.3. Short Duration Rainfall Extremes

Through explicit representation of convective storms such as thunderstorms, CPMs are expected to substantially improve the representation of high intensity precipitation over short time-periods. Observational studies have indicated that the intensity of the most extreme precipitation rates is increasing due to climate change. In other regions of the world, it has been demonstrated that CPMs are able to capture this increase, and that convection-parameterised RCMs and GCMs cannot. Therefore, the representation of short duration rainfall extremes in CPMs is a substantial motivator for convection-permitting climate projections.

In this paper, we focus on the multi-year mean of annual maximum hourly precipitation (RX1H) as the main quantifier of short duration high intensity rainfall. This metric is the mean of the highest rain-rates in each of the ten years in the modelled time-period and provides a balance between considering extreme rainfall and selecting a metric that is reasonably well sampled in the short 10-year simulations.

Figure 8 compares RX1H in the three models to automatic weather station observational data. Model data is interpolated to station locations using a nearest-neighbour remapping. Figure 8 indicates that observed and BARPA-C based RX1H can reach levels of up to 80 mm/hr in northern and east-coast Australia. By contrast, in BARPA-R, RX1H is capped at about 40 mm/hr. While BARPA-R consistently underestimates RX1H across northern and eastern Australia, BARPA-C\_SN and BARPA-C\_FR show a mix of positive and negative biases, indicating no systematic directional bias overall. Spatial patterns of RX1H also differ between BARPA-R and BARPA-C - a clear zone of elevated RX1H stretches all the way along the Queensland and NSW coasts in BARPA-C that is not present in BARPA-R. This suggests that BARPA-C provides added value in the representation of RX1H that could not be reproduced simply by scaling up BARPA-R.

BARPA-C\_FR and BARPA-R\_SN show very few differences over land. Over the ocean, BARPA-C\_FR shows slightly reduced extreme rain rates, likely due to the decreased frequency of tropical cyclones. BARPA-C shows a substantial improvement in the



representation of short-duration rainfall extremes, meeting Benchmark 2 described at the start of section 3.

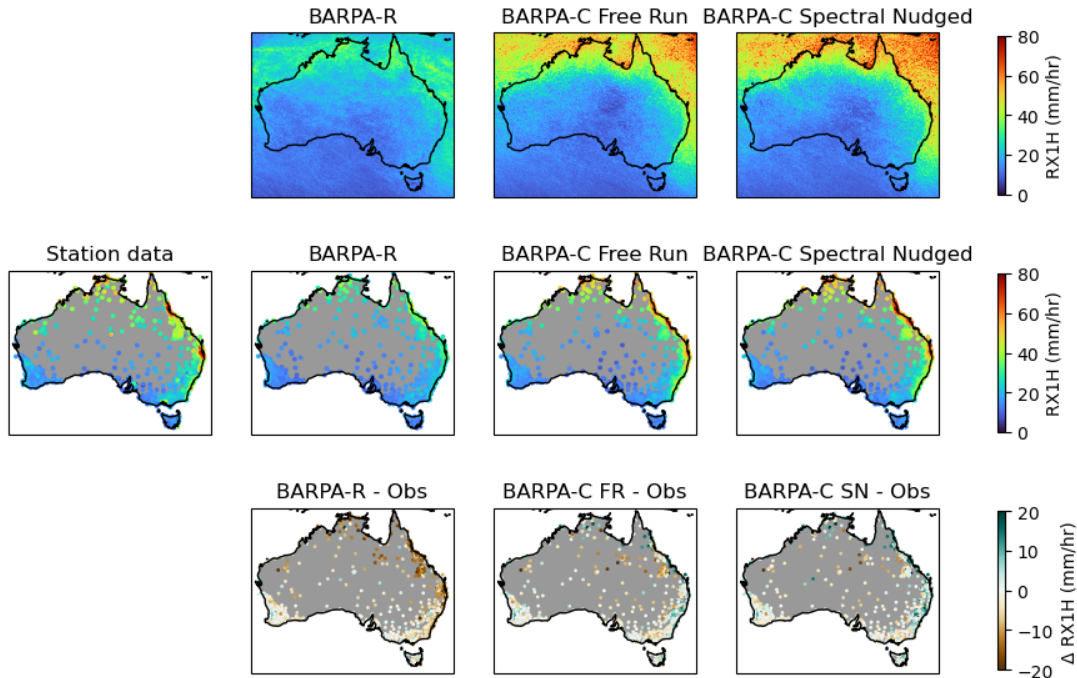


Figure 8: 10-year Annual mean of hourly maximum precipitation rate (RX1H) across BARPA-R, BARPA-C\_FR and BARPA-C\_SN, compared to station data. Top row: full fields of modelled RX1H. Middle row: observed RX1H (left) and RX1H interpolated to station locations using nearest-neighbour regriding. Bottom: bias in RX1H at station locations.

The improvement in the representation of hourly extreme rainfall in northern and eastern Australia can also be seen through comparison with radar-based observations. Three radars at Gove in the Top End, Mackay in north Queensland and Terrey Hills in Sydney have been selected based on their high rainfall climatologies and the consistency of their long-term mean rainfall with AGCD. Figure 9 shows the distribution of hourly rain rates across the simulation period, compared to these radars. Both BARPA-C\_FR and BARPA-C\_SN show good agreement with radar observations at capturing rain-rates between above 50 mm/hour, while BARPA-R shows a unphysical cut-offs between 45 and 60 mm/hour. BARPA-C\_FR slightly underestimates the radar observations in Mackay and Gove. In Sydney, more moderate rain-rates between 1 and 20 mm per hour are consistently overestimated by all BARPA models, consistent with the wet bias reported by Bush et al., (2024).

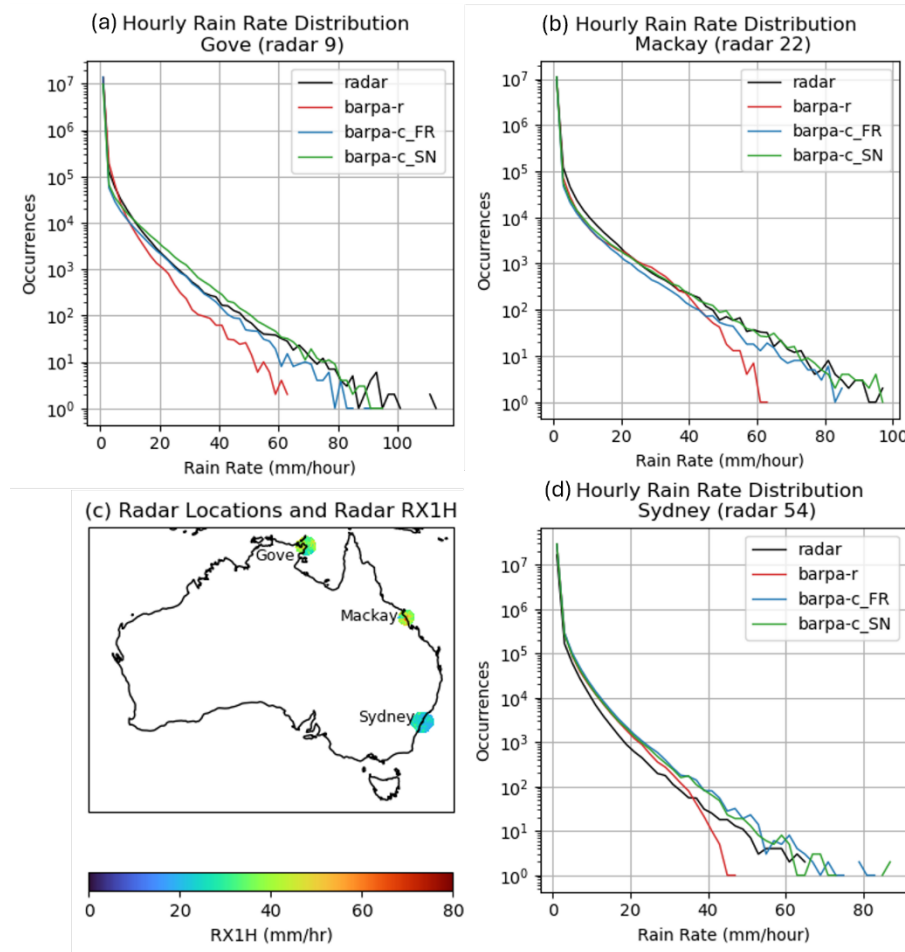


Figure 9: Modelled and observed distribution of hourly rainfall at (a) Gove, (b) Mackay and (d) Sydney Terrey Hills radars. Panel (c) shows a map of radar location, with radar-based RX1H shown in colours. Radar and BARPA-C data have been regridded conservatively to the BARPA-R grid, and only time-steps with valid radar data are considered.

### 3.4. Tropical Low-Pressure Systems

Tropical cyclones are a key weather hazard for the northern Australian region, often bringing heavy rainfall, flooding and extreme winds upon landfall. As convectively driven weather-systems, tropical cyclones are poorly represented in convection parametrised climate models, and so CPMs are expected to improve the representation of tropical cyclones.

For the purposes of this early analysis, a simplified algorithm has been applied to identify the instantaneous locations of tropical low-pressure systems. This algorithm divides the BARPA-C tropical domain (north of 23 S) into three regions: East, West and North, separated by meridians at 125 E and 142 E. It then identifies tropical low-pressure systems as absolute minima of daily-mean sea level pressure (PSL) in the interior of each region. Only systems with central pressures less than 995 hPa are retained. This approach only identifies the strongest event at each day in each region. However, based



on a visual inspection of PSL Hovmoller plots, the small size of the three regions ensures multiple cyclones are never present in any region at the same time.

As this algorithm is not a wind-based classification system like the Australian tropical cyclone intensity scale or the Saffir-Simpson scale, not all identified systems will be classified as tropical cyclones. Therefore, we refer to storms identified using this algorithm as tropical low-pressure systems rather than tropical cyclones.

Figure 10 presents the track frequencies of tropical low-pressure systems identified, compared to IBTrACS. Daily storm locations are shown as a scatterplot in the top row with minimum pressure indicated by dot colour, and for more quantitative comparison as a binned frequency count map in the middle row. The model biases of the frequency counts from IBTrACS is shown in the final row.

All three models overestimate the tropical cyclone frequency in the south-east of the maps, off the coast of south-east Queensland. BARPA-R shows an overly high number of inland tropical low-pressure systems, suggesting that it struggles to correctly simulate lysis following landfall. BARPA-C\_FR simulates too few tropical low-pressure systems over northern Australia, likely due to the northward shift in the monsoon shearline discussed in section 3.2. This is a concern since land-falling cyclones in Northern Australia are a key hazard for ACS. However, BARPA-C\_SN shows very good performance, with a realistic distribution of cyclones over the Top End. It does show a reduction in storms over the Kimberly, but this is improved compared with BARPA-C\_FR.

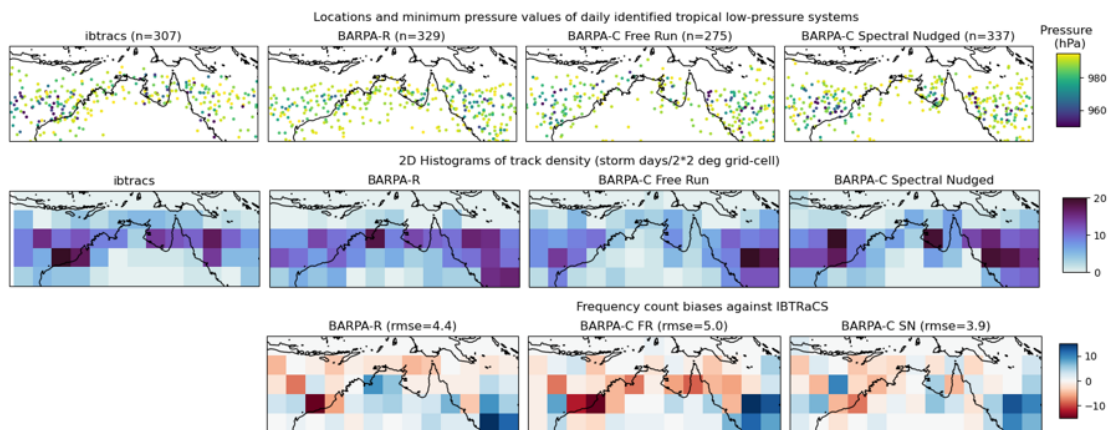


Figure 10: Tropical cyclone track frequencies across BARPA-R, BARPA-C\_FR and BARPA-C\_SN compared to IBTRaCS. Top row: scatterplot of all cyclone locations derived from daily mean data, with minimum pressure indicated by colours. Middle row: heatmap frequency plots of cyclone locations on 4\*4 degree grid. Bottom row: difference of frequency heatmaps between BARPA models and IBTRaCS.

The distribution of intensities of the tropical low-pressure systems is shown in Figure 11. Again, no attempt has been made to 'track' the tropical low-pressure systems for this early analysis, and instead a datapoint is presented for each cyclone day. This figure indicates that BARPA-R struggles to simulate tropical low-pressure systems with central pressures deeper than 955 hPa, while both BARPA-C simulations are able to reproduce



a realistic number of deep systems. Over the simulation period, a total of 24 days featured tropical low-pressure systems with central pressures deeper than 955 hPa in observations. In comparison, BARPA-C\_SN simulated 19, BARPA-C\_FR simulated 13, and BARPA-R only one. The reduced number of deep systems in BARPA-C\_FR is likely due to the overall bias in the number of systems shown in Figure 10.

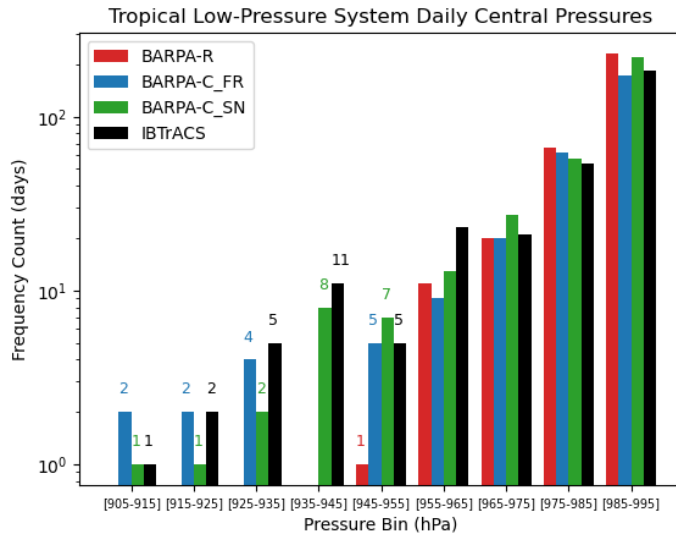


Figure 11: Frequency count of days with tropical low-pressure systems identified, against central pressure. The y-axis is log-scaled. Frequency counts below 955 hPa are annotated on the figure.

Overall BARPA-C\_SN performs very well at simulating the frequency of high-intensity tropical low-pressure systems in the Australian region. Spectral nudging was able to address a low-frequency bias in the total cyclone count in northern Australia.

## 4. Trial Assessment

This section describes the system trials run during the development of the BARPA-C configurations described above. These trials were designed to test technical aspects of the system, evaluate speed and CPU use and timing statistics, and to test the sensitivity to proposed system changes additional to RAL3 as described in section 2. The trials described in this document are listed in table 1 below.

Table 1: Targeted Trial descriptions

	Trial	Period/ driving data	Description	Domain/ Grid-cells (nx xny)
Boundary Width (Sec 4.1)	Trial_BC1	2013 ERA5	Large domain year-long trial	AUS-3 1360x1036
	Trial_BC2	2013 ERA5	Small domain year-long trial	AUS-1 1360x1176
Land Use (Sec. 4.2)	Trial_LU_CCI	2013 ERA5	Large domain year-long trial	AUS-3 1360x1036
	Trial_LU_AA	2013 ERA5	New Land ancils, Proposed domain	AU-M 1348x1068

Urban Land Surface (Sec. 4.3)	Trial_urb_ctrl	Jan/Feb 2098 CESM2	Future period, 365 day calendar	AU-M 1348×1068
	Trial_urb_lai	Jan/Feb 2098 CESM2	Future period, 365 day calendar, LAI fix	AU-M 1348×1068
	Trial_urb_infiltr	Jan/Feb 2098 CESM2	Future period, 365 day calendar, LAI fix, infiltration fix	AU-M 1348×1068
Spectral Nudging (Sec. 4.4)	Trial_SN_ctrl	Sep 2012 – Mar 2018 ERA5	Free Run	AU-M 1348×1068
	Trial_SN-e1	Sep 2012 – Mar 2018 ERA5	Nudging lengthscale: L=1270 km Nudging timescale: e=1 hour	AU-M 1348×1068
	Trial_SN-e12	Sep 2012 – Mar 2018 ERA5	Nudging lengthscale: L=1270 km Nudging timescale:e=12 hours	AU-M 1348×1068

The assessments performed were as follows:

- A. Boundary width: comparison of trials with different domain sizes.
- B. Land use: comparison of trials with different land-use ancillaries
- C. Urban Land surface: resolution of a bug fix causing overly wet soil moistures in urban areas
- D. Spectral nudging: selection of appropriate parameters for the spectral nudging in BARPA-C SN.

## 4.1. Boundary Widths

The domain presented in Figure 1 was selected so that the domain boundaries were sufficiently far from Australian landmass so that boundary effects were not present on the continent. Two trials, referred to here as trial\_BC1 and trial\_BC2, were conducted to determine the size of the required buffer zone around Australia.

These trials were run on different domains, with trial\_BC1 having its southern boundary at 45S, and trial\_BC2 having its southern boundary located at 51S. It was assumed that the impact of the southern boundary was negligible in trial\_BC2 north of 45S. Ten daily two-dimensional variables relating to precipitation, near-surface wind, cloud and near-surface temperature were then selected, and their distributions across time and longitude were computed for each trial and for each latitude band between 45S and 30S. Perkins Skill Scores (PSS), which measure the difference between two distributions, were then calculated for each latitude between the two trial distributions. These PSS values are shown in blue in Figure 12. Declines in the PSS values at higher latitudes are then attributed to boundary effects of the southern boundary of trial\_BC1.

A visual inspection of Figure 12 indicates that boundary effects are negligible at 42S, which is 3 degrees north of the southern boundary. Therefore, the minimum necessary buffer around the Australian continent was determined to be 3 degrees. This is significantly wider than the relaxation zone (0.48 deg), over which the boundary forcing is applied, and the blending zone (0.88 deg) for blending the orographic heights on the global and regional grids. The southern boundary of the BARPA-C domain is therefore set to 46.7S, which is 3 degrees south of Tasmania's southernmost point.

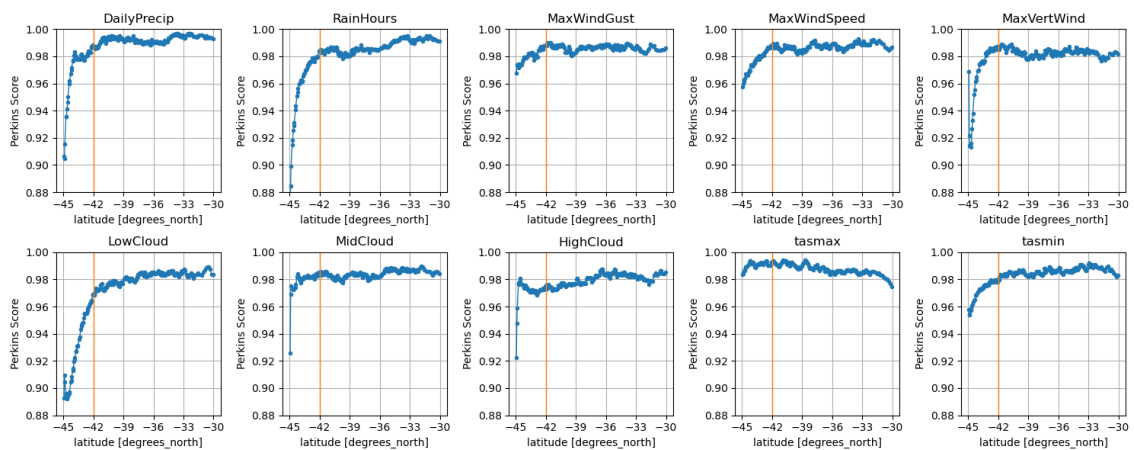


Figure 12: Boundary effects on key variables by latitude.

## 4.2. ACCESS-A Land Use Ancillaries

As described in section 2.2, BARPA-C uses an updated land use dataset created for use in convection permitting MetUM atmospheric modelling in Australia. The impact of the updated land use dataset was investigated in the comparison of trial\_LU\_CCI and trial\_LU\_AA. The changes in land use type associated with the ACCESS-A ancillaries describes above are shown in Figure 13 together with the eight National Resource Management (NRM) cluster regions used in the analysis. These figures show the grid-cell transfer fractions between the pairs of land use categories with significant transfers. These include:

- changes between shrubs, C3 grass and C4 grass, caused by interannual variability between the CCIv1 and CCIv2 datasets and by the new grass partition dataset;
- transitions from inland water to bare soil, caused by reclassification of Australian inland lakes, which are typically dry lakes, as bare soil; and
- transfers to all other land use types from Urban, caused by the use of the WorldCover dataset.

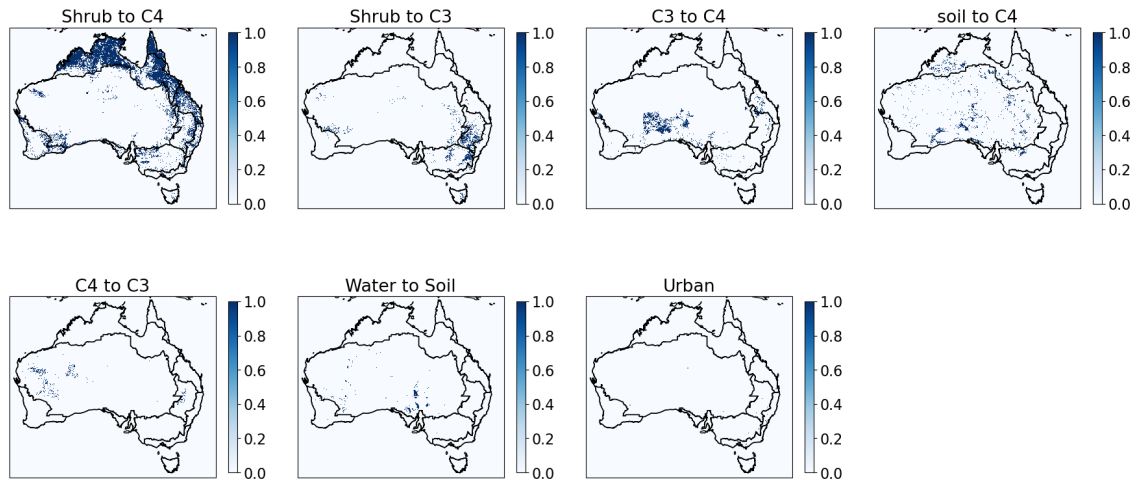


Figure 13: Fraction of each grid-cell undergoing land use type transformation for each major land use transformation pair as per text. The final panel provides a key for the NRM spatial clusters.

In Figure 14, the median changes of average tasmin, tasmax and diurnal temperature range in each NRM cluster and each transfer pair is shown. These figures demonstrate that removing inland water in the rangelands cluster increases diurnal temperature range by about 6°C, and that reducing urban fraction reduces tasmin by about 1.5 °C. Soil to C4 decreases minimum temperature by about half a degree. The remaining changes are small and unlikely to be robust to internal variability. For example, the C4 to C3 change is associated with the same sign of change as the C3 to C4 change, indicating that these differences between the simulations are caused by something other than the land use change.

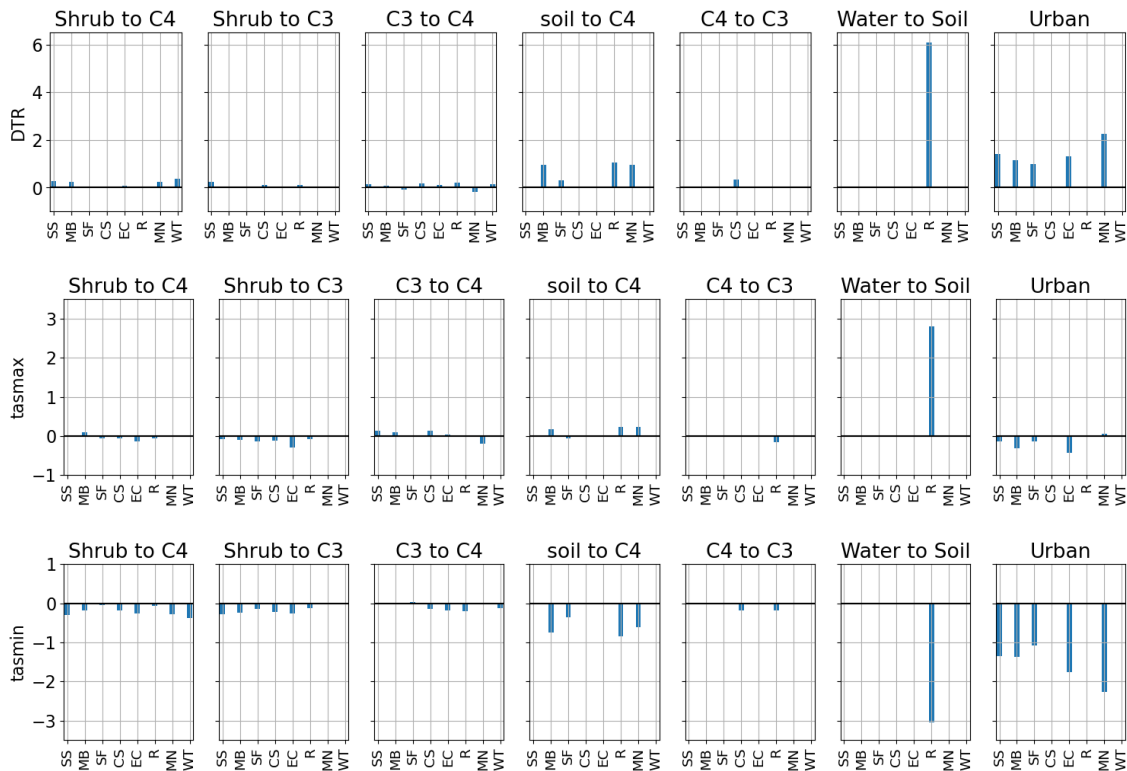


Figure 14: NRM Cluster-mean change in diurnal temperature range, (top row) tasmax (middle row) and tasmin (bottom row) in the region of each land use type transform pair (as per text) between trial\_LU\_CCI and trial\_LU\_AA.

To classify the impact of the land use type update on soil moisture, Figure 14 presents time-series of the average soil moisture in trial\_LU\_CCI and trial\_LU\_AA in all combinations of transfer pairs and NRM clusters that show substantial deviation between the trials. Soil moisture is assessed in the top two soil levels only. Here, 'substantial deviation' is judged to occur when the median change in the top layer exceeds  $0.5 \text{ kg/m}^2$ . In urban areas, trial\_LU\_AA shows faster dry down rate than trial\_LU\_CCI. This is associated with partial resolution of the urban wet bias issue, further examined in section 4.3. The conversion of dry lakes from inland water to soil results in faster dry down and higher infiltration in trial\_LU\_AA than trial\_LU\_CCI.

The remaining comparisons show only minor differences. Panels (a) to (e) indicate deviations between the timeseries between March and May, however this is likely due to divergence in incoming rainfall due to modelled internal variability. In panels (a), (b) and (c), trial\_LU\_AA appears to have slightly increased infiltration over trial\_LU\_CCI while dry down rates appear unchanged.

Overall, the 'water to soil' and 'urban' changes are both judged to be beneficial, while the remaining changes are considered neutral. Therefore, the ACCESS-A ancillaries have been adopted for BARPA-C. The urban change is further examined in the following section.

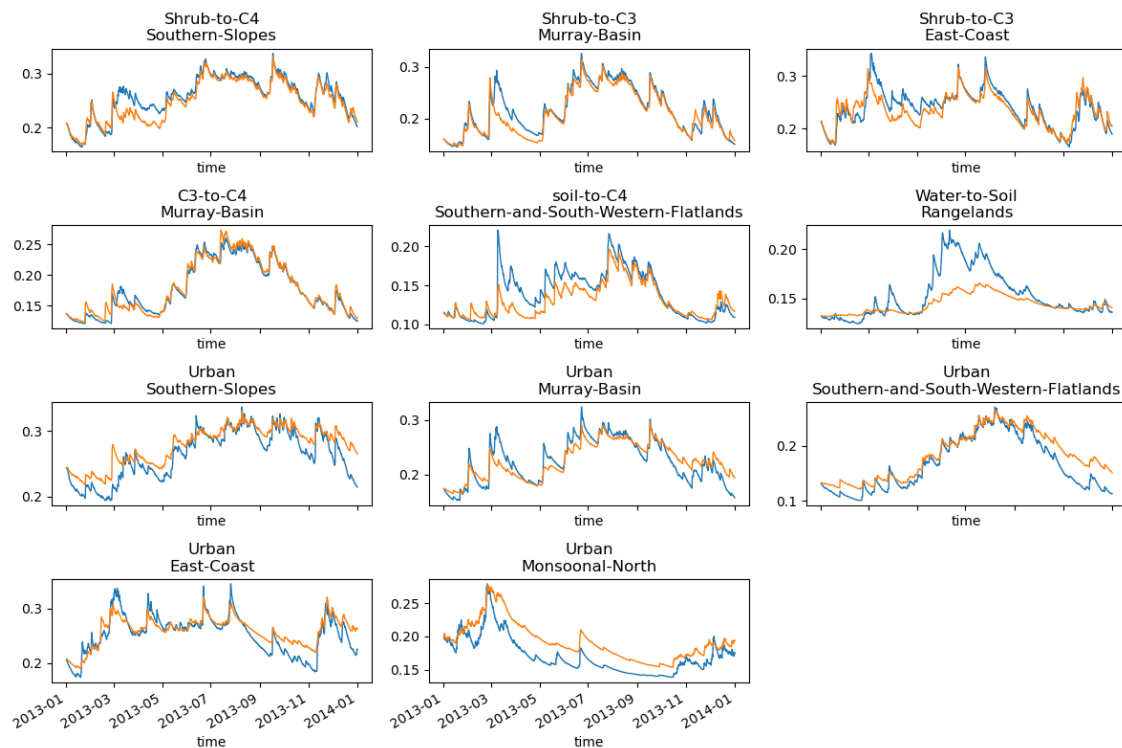


Figure 15: Timeseries of NRM cluster mean soil moisture in regions where the land-use type is updated (as per Figure 2). Soil moisture is summed across the top two soil model layers and has units of kg/m<sup>3</sup>. Only cluster/land use transformation pair combinations with a substantial change in soil moisture are shown. trial\_LU\_AA is shown in blue, while trial\_LU\_CCI is shown in orange.

### 4.3. Urban Land Surface Modifications

This section investigates the high sensitivity of the urban soil moisture to the land-use type described in section 2.2. This sensitivity derives from the partial resolution of a long-standing urban wet soil moisture bias first identified in the ACCESS forecast models, documented at [485](#). Spuriously wet urban soils in free-running simulations were present in BARPA-R and derive from three issues:

1. The leaf area index values (LAI) in the MODIS source dataset are masked due to technical satellite retrieval challenges in built-up areas. By default, these masked values are treated as zeros, prohibiting transpiration out of each grid-box.
2. The urban tile component of each grid-cell allows for a small amount of water infiltration into the gridbox, but not for evaporation out of the grid-box.
3. The urban land cover fraction is unrealistically high in many datasets, including IGBP, CCI and CCIv2. This exacerbates the second issue by reducing the grid-cell fraction that is capable of evaporation.

Issue 3 was resolved in trial\_LU\_AA by replacing the CCIv2 urban tile fraction with a dataset derived from WorldCover, as described in section 2.2. This allows for more evaporation to occur out of the urban tiles, resulting in the faster dry down rates visible



in Figure 15. Trial\_urb\_orig, trial\_urb\_lai and trial\_urb\_infilt were designed to test the impact of resolving issues 1 and 2 on the urban soil moisture and near-surface temperatures.

As the urban soil moisture wet bias is caused by moisture being unable to leave the soil after a saturation, it is most apparent during extended dry periods. Therefore, the time-period for trial\_urb\_orig, trial\_urb\_lai and trial\_urb\_infilt was chosen to cover a dry-spell in Sydney based on BARPA-R. To additionally stress-test the model at simulating future climates, and to test the 365-day calendar functionality, the dry period selected was January and February, 2098, with boundary conditions derived from the BARPA-R of CESM2, a CMIP6 GCM produced by NCAR.

As per table 1, trial\_urb\_orig was designed to be the control trial, matching the configuration of trial\_lu\_AA for the 2098 time-period. trial\_urb\_lai aimed to resolve issue (1) in the table above by infilling the leaf area index. Infilling was achieved by identifying the region where LAI is masked in the original MODIS data and applying a nearest-neighbour approach. Finally, trial\_urb\_infilt addressed issue (2) by setting the infiltration enhancement factor to zero on urban tiles, as well as infilling LAI as per trial E. This value originally had a value of 0.1 on urban tiles, compared to a value of 2 on grass and shrub tiles and 4 on tree tiles.

For each trial, the panels of Figure 16 compares of 15-day time-series of 6-hourly soil moisture averaged over the Sydney urban area (urban time fraction >0.5) and averaged over the non-urban region surrounding Sydney (urban time fraction < 0.2). As rainfall in these two regions is well correlated, these timeseries should be similar to each other in the absence of a soil moisture bias. Spikes in these time-series represent rainfall events, where the soil moisture reaches saturation if sufficient rainfall occurs. The soil moisture biases manifest as a reduction of the dry down rate following the rain event and plateauing of the urban soil moisture to higher asymptote than the adjacent region.

Both BARPA-R and trial\_LU\_CCI show substantial wet biases. Trial\_LU\_AA and trial\_urb\_orig show a substantial improvement in the soil moisture in the top soil level, deriving from the restored ability of the soil moisture to evaporate from the first model layer. However, soil moisture in the second model layer remains too wet. This reflects the inability of the soil model to lose water to transpiration, which typically removes moisture from the lower model levels, the 'root zones' where plant roots extract water. The LAI infilling fix (trial\_urb\_lai) resolves this by restoring transpiration, so that the soil moisture in the second soil level is comparable across urban and adjacent non-urban areas.

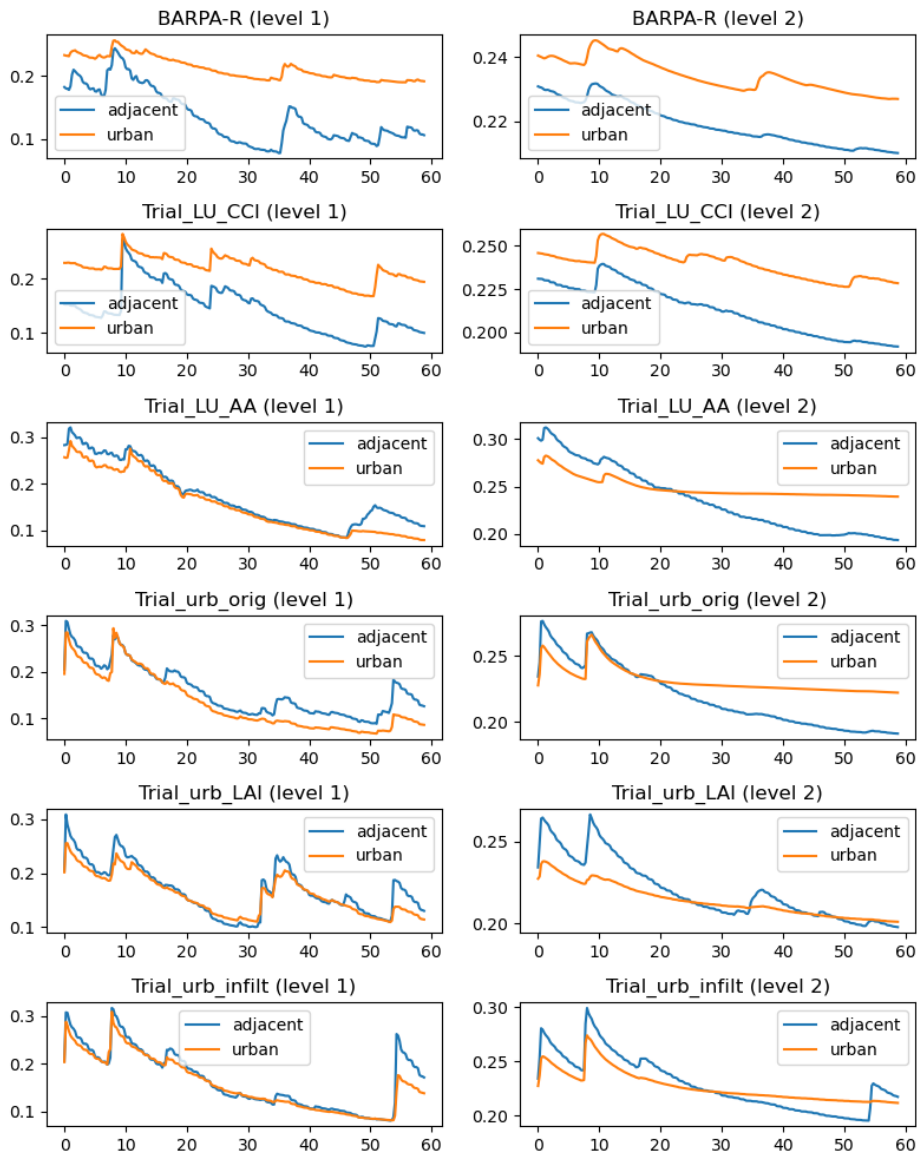


Figure 16: Time series of urban soil moisture in Sydney in BARPA-R and in the urban and land-use trials. Orange: average across region with urban tile fraction >0.5. Blue: average across bushland adjacent to Sydney (urban tile fraction <0.2).

Finally, trial\_urb\_infiltr is designed to prevent the infiltration of soil moisture into the urban tile component of each grid-box. In previous trials, infiltration is allowed but evapotranspiration prevented on the urban component, meaning that the non-urban component of the tile must overcompensate to remove moisture from urban areas. This overcompensation is possible because soil moisture is shared across tiles. However, this trial showed no substantial improvement over trial\_urb\_lai, and showed an increase in total infiltration in the urban areas compared to the non-urban areas associated with

the rainfall event, a finding that is not fully understood<sup>1</sup>. Unlike the other trials which only modify ancillary files, trial\_urb\_infil represents a deviation from the RAL3.2 configuration of the regional MetUM as it includes a namelist change. **Therefore, the decision was made to proceed with the trial\_urb\_lai configuration.**

#### 4.4. Spectral Nudging

Table 2: Spectral nudging parameters across regional modelling studies. Where a length-scale was recommended by the study, it is indicated in bold.

Reference	Model	Model grid-spacing	Tested Length-scales ( $L$ )	Tested time-scales ( $\epsilon$ )
Uhe and Thatcher (2015)	MetUM	150km	191km <b>640km</b> <b>1270km</b> 3000 km	1-hr, 6-hr
Schroeter et. al. (2024)	CCAM	11km	2135 km <sup>2</sup>	4-minute (timestep)
Huang et. al. (2021)	WRF	10km	1000 km	54 mins, 6:20-hr
Yang et. al. (2019)	WRF	25km	<b>500km 1000km</b> 2000km	1-hr, 3-hr
Gomez et (2017)	WRF	36km	170km, ... <b>1000km</b> , ... 4000km	54 mins

Nudging has been used in climate modelling to constrain models to a driving dataset for many years. Nudging in global models is used to constrain the circulation to observations to allow smoother comparison with in-situ measurements, particularly when studying tracer fields such as aerosols (Fiddes et al., 2022). Spectral nudging is used in downscaling to constrain large length-scales while leaving smaller length-scales free to evolve. In variable-resolution global climate models such as CCAM, it can be the only atmospheric source of driving model input (Schroeter et al., 2024; Thatcher & McGregor, 2009). In limited area modelling, spectral nudging has been applied in a range of locations, including the Tibetan Plateau (Huang et al., 2021), East Asia (Yang et al., 2019) and Western Europe (Gómez & Miguez-Macho, 2017) using the Weather Research and Forecasting (WRF) model.

<sup>1</sup>As per all short trials considered in this study, rainfall is sensitive to internal variability and trial\_urb\_infil did feature a stronger rain event over Sydney, which may have contributed to this higher infiltration.

<sup>2</sup> (Schroeter et al., 2024) describes the nudging length-scale as 3000 km, however this refers to a slightly different formulation of the nudging equation. 2135km has been derived as the equivalent for equation 1, and confirmed through private communication with the authors.



The nudging length-scale selected for BARPA-C has been chosen through a literature review of previous studies using spectral nudging for climate-scale simulations. The papers considered recommend a range of length-scales between 500km and 1300km. For the sake of minimising the impact of nudging and allowing small length-scales to develop independently, the nudging length-scale was set to be 0.2 radians, equivalent to **1270km**.

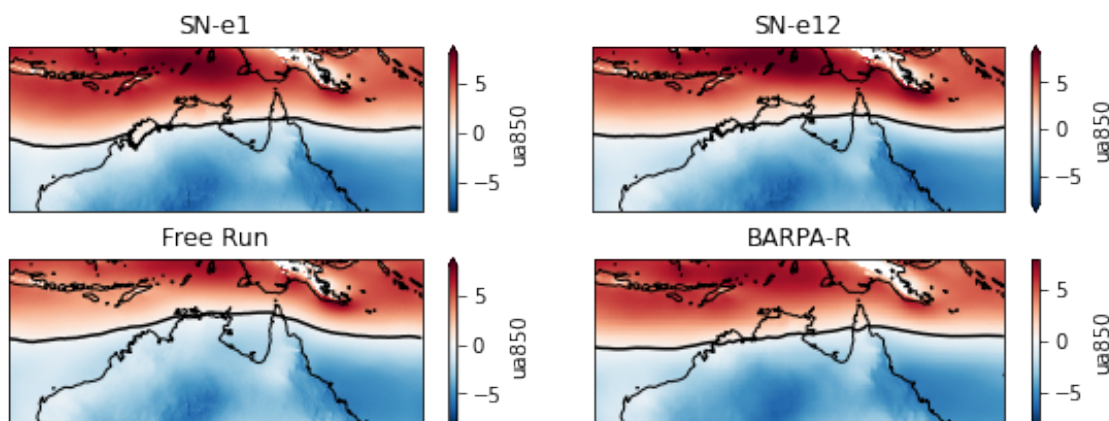


Figure 17: DJF-mean 850 hPa winds as per figure 5 but for the spectral nudging trials.

The nudging timescale was chosen through the comparison of three 5-year long trials with no nudging (trial\_SN\_ctrl), strong nudging using a 1-hour nudging timescale (trial\_SN-e1) and soft nudging using a 12-hour nudging timescale (trial\_SN-e12) as described in Table 1. Of these, trial\_SN\_ctrl and trial\_SN-e12 were extended into BARPA-C\_FR and BARPA-C\_SN considered in section 3 above.

As shown in Figure 17, both spectral nudging trials were found to restore the monsoon winds to match BARPA-R levels, with the monsoon trough passing over Northern Australia close to its location in BARPA-R. However, daily extreme rainfall was adversely impacted by the strong spectral nudging applied in SN-e1, with a wet bias of mean monthly maximum daily rainfall (RX1D) emerging in northern Australia in excess of that present in BARPA-R (Figure 18). Further investigation revealed that this was due to the spin-up of unrealistically strong tropical low-pressure systems in the strongly nudged experiments. Whereas the deepest Australian-region tropical low-pressure systems observed in the IBTrACS record between 2013 and 2022 had a central pressure of 915 hPa, trial\_SN-e1 spun up several systems with central pressures of order 880 hPa. In the shorter trial period, trial\_SN\_e1 had 2.7 times more intense tropical low-pressure systems deeper than 935 hPa compared to observations.

This excess of tropical cyclones negatively impacts the representation of hazardous climate extremes. As the ACS is focussed towards representing climate hazards, this was deemed to be a serious issue. Furthermore, the excess of very strong tropical low-pressure systems that the strong spectral nudging may be introducing computational instabilities into the model. **Therefore, the decision was made to proceed with the soft nudging setup of SN-e12.**



DJF RX1Day: Dec 2012-Feb 2018

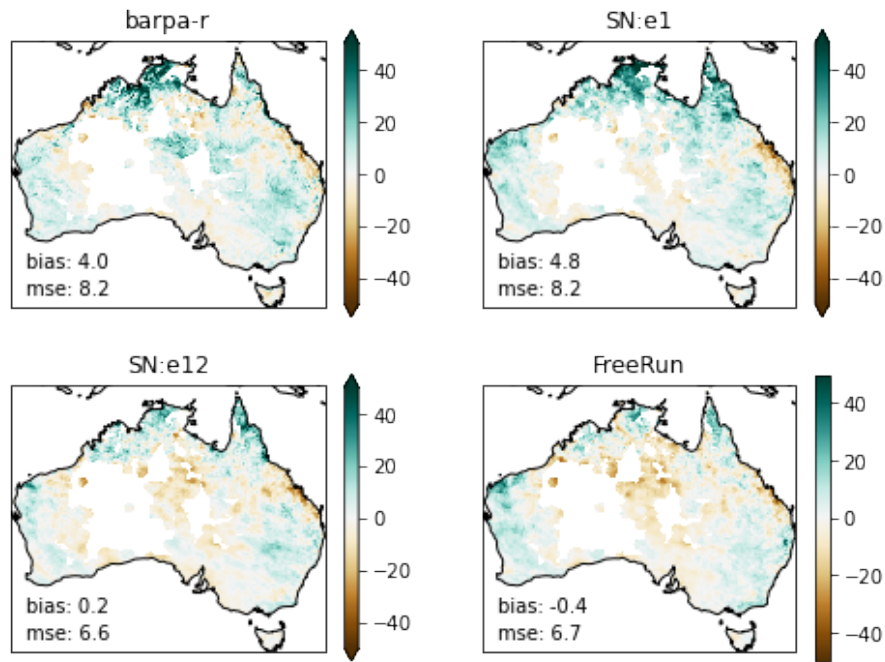


Figure 18: RX1D bias against AGCD. All datasets were regridded to the BARPA-R grid before index calculation.

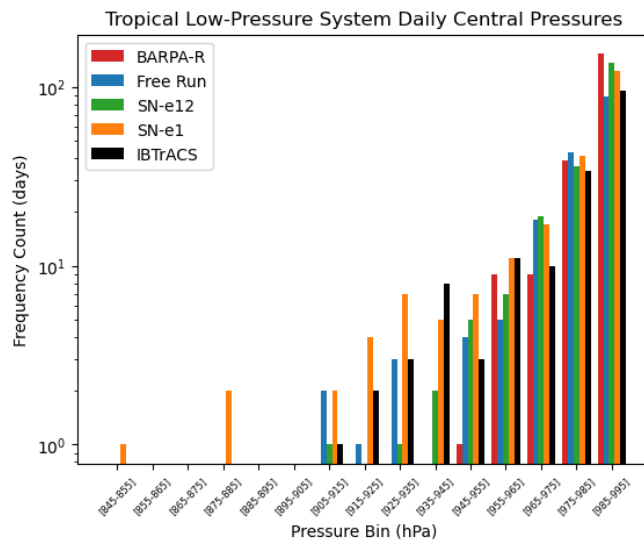


Figure 19: Tropical cyclone intensities as per figure 11 for spectral nudging trials.



## 5. Discussion and Conclusions

This work represents the first ever Australia-wide convection permitting simulations conducted on climate-timescales. It has benefited from substantial model development unifying the regional MetUM science configurations across tropical and midlatitude domains. These simulations show a step-change improvement in the representation of convective hazards such as tropical cyclones and short duration high-intensity rainfall compared to coarser convection-parametrised models.

### 5.1. Performance Benchmarks

This paper has presented two prototype model configurations for convection-permitting climate modelling with the Bureau's BARPA climate model, labelled BARPA-C\_FR and BARPA-C\_SN. In section 3, the mean-state and representation of two key hazards in BARPA-C was assessed. Performance was benchmarked against two criteria:

**Benchmark 1:** BARPA-C should not significantly degrade the mean-state compared to BARPA-R, and

**Benchmark 2:** The representation of hazard-relevant climate extremes that are intrinsically linked to convective processes is substantially improved in BARPA-C compared to BARPA-R.

Mean-state representation of near-surface air temperatures met benchmark 1 in a straight-forward fashion. However, while improvements to the rainfall climate were present, particularly in coastal southern Australia and during the Australian spring, mean-state precipitation over land was degraded for Northern Australia from December to February. This resulted in a misrepresentation of the Australian monsoon circulation in BARPA-C\_FR. BARPA-C\_SN was able to restore the mean-state of the monsoon circulation but retained a dry-bias over land.

In consideration of benchmark 2, the representation of extreme hourly rainfall and tropical cyclones was assessed. Both BARPA-C configurations were able to substantially improve on the BARPA-R in the representation of RX1H, the multi-year mean of the annual highest precipitation rate, as compared to station observations, particularly in Eastern and Northern Australia.

BARPA-C\_SN showed a skilful representation of the tropical low-pressure system climatology by well simulating both the spatial distribution and the intensities of cyclone-like systems in the Australian region. BARPA-C\_FR was also able to simulate intense tropical low-pressure systems, but suffered a bias in the total cyclone count due to the mean-state circulation bias in the monsoon westerlies. In contrast, the benchmark BARPA-R was not able to simulate deep tropical low-pressure systems with sea level pressure minima below 950 hPa.

Overall, BARPA-C\_SN was deemed to be the best configuration considered due to its representation of hazard-relevant climate extremes, despite the degradation of the mean-state precipitation over land in northern Australia.



The use of suitable benchmarks during the trial phase of model development is critical for decision making around model configuration acceptance and use for production-quality climate projections. This is particularly important given the compute cost of running high resolution models, and for the assessment of new approaches for the generation of km-scale projections.

## 5.2. Lessons learned for future trials

The development phase of BARPA-C used 10-year, 1-year and 2-month long trials to select a finalised configuration. All trials were nested inside of BARPA-R. Although useful for assessing the sensitivity of BARPA-C to various configuration settings, it was not possible to compare the shorter trials to observations due to sampling uncertainty. This was in part because the interannual variability of BARPA-R was out of sync with observations, particularly in the northern Australian monsoon as illustrated by Figure 6.

As such, nesting within BARPA-R adds an additional degree of complication that is unnecessary in the evaluation experiments. Future evaluation trials should therefore be nested directly in either regional reanalysis (BARRA-R2, Su, Rennie, et al., 2022) or ERA5 global reanalysis, so that interannual variability of tropical circulation may align with observations. This is in line with CORDEX protocols (Giorgi et al., 2009), which require evaluation runs to be use realistic boundary input. GCM downscaling experiments should continue to use BARPA-R as an intermediate nest in order to step down from the significantly coarser (~100 km) grid-spacings.

The 10-year trials appear to be sufficiently long for evaluation of mean-state phenomena against observations. However, we note that based on the emergence of the dry bias in BARPA-C\_SN after 4 years, substitution with a shorter time-period would not be advised.

## 5.3. Limitations and future plans

This work has revealed a significant dry bias in northern Australian precipitation over land in both BARPA-C simulations. This bias was not present in BARPA-R. The presence of the dry bias in BARPA-C\_SN suggests that it is not a consequence of atmospheric circulation biases, but rather that it intensifies through circulation feedback. This dry bias prevented the satisfaction of the first applied model benchmark, that mean-state biases would not be significantly degraded compared to BARPA-R.

Future model development will focus on attempting to reduce this dry bias. However, biases will never be fully removed from dynamical climate models. Furthermore, limited area models inherit additional biases from their driving datasets, particularly when downscaling GCMs (Jiang et al., 2025). Therefore, bias correction techniques are required to prepare CPM outputs before use for climate services or impact modelling.

As discussed in section 1.2, storm processes are not fully resolved in kilometre-scale models, and therefore these models operate in a convective grey zone. This is particularly important in models with 4-km grid spacing, as compared to 1 or 2-km (Stein et al 2014, Potvin 2015). While BARPA-C can explicitly represent a form of deep convection, small-scale and shallow convection is only crudely represented. The



development of scale-aware grey zone convection schemes, which parametrise unresolved convection while allowing grid-scale convection to evolve naturally has the potential to resolve these problems (Tomassini et al., 2023). These convection schemes will differ substantially from traditional mass-flux convection schemes, which tend to prevent resolved convection from occurring by removing environmental CAPE (Gregory and Rowntree, 1990).

Potential avenues for exploration that may improve on the Northern Australian dry bias include microphysics schemes, the inclusion of scale-aware convection schemes, and land surface parameters. Following the findings of section 5.2, short trials nested directly within ERA5 may assist in providing clarity around the source of the dry bias through closer coupling with observations. In particular, the land-use changes discussed in section 4.2 will be revisited with these findings in mind. However, there is no guarantee of that any of these methods will reduce the dry bias.

Furthermore, when downscaling climate projections, mean-state biases can be inherited from both the downscaling model configuration and the driving GCM. This was illustrated for BARPA-R by Jiang et al., (2025) and is expected to persist into BARPA-C. Therefore, the performance of BARPA-C at downscaling ERA5 may be modified when downscaling GCM simulations, and this should also be assessed.

A decision has therefore been made to proceed with a limited set of GCM downscaling experiments with BARPA-C. These experiments will be focused for research use only. Two models have been selected: EC-Earth3 and ACCESS-ESM1.5 based on their divergent rainfall projections for Australia (Grose et. al., 2023). These models feature the wettest and driest future projections of the BARPA-R ensemble. A historical (1995-2004) and mid-century (2050-2059) time-slice will be downscaled by each model, and the moderate-high emissions scenario shared socio-economic pathways (SSP) 3-7.0 has been selected for downscaling.

The current version of BARPA-R and BARPA-C represents a good basis for improving future versions of high-resolution projections over Australia. While some issues remain in mean-state rainfall in the tropics, the representation of convective hazards such as intense tropical low-pressure systems and short duration high intensity rainfall are much improved over the previous generation of BARPA. Next, this framework will be applied to produce convection-permitting downscaled climate projections.

## Acknowledgements

This work was supported by the Australian Climate Service (ACS). We acknowledge valuable inputs from following people: M. Thatcher (CSIRO) on advice on climate modelling and spectral nudging; C. Short (UKMO) for advice on convective-scale modelling with the UM; B. Trewin and Joshua Soderholm (BOM) for access to observational datasets, S. Tian, I. Dharssi and C. Rudiger (BOM, ECMWF) for advice on land-surface processes, and M. Grose and A. Dowdy (CSIRO, UoM) for input on experimental design. We thank Acacia Pepler and Vinod Kumar for helpful feedback which has improved this manuscript.



This work was undertaken with the assistance of resources and services from National Computational Infrastructure (NCI), which is supported by the Australian Government. As an ESGF node, NCI manages the CMIP collections as well as other ESGF data sets, used in this work.

## References

- Bao, J., Sherwood, S. C., Alexander, L. V., & Evans, J. P. (2017). Future increases in extreme precipitation exceed observed scaling rates. *Nature Climate Change*, 7(2), 128–132. <https://doi.org/10.1038/nclimate3201>
- Belušić Vozila, A., Belušić, D., Telišman Prtenjak, M., Güttler, I., Bastin, S., Brisson, E., Demory, M. E., Dobler, A., Feldmann, H., Hodnebrog, Ø., Kartsios, S., Keuler, K., Lorenz, T., Milovac, J., Pichelli, E., Raffa, M., Soares, P. M. M., Tölle, M. H., Truhetz, H., ... Warrach-Sagi, K. (2024). Evaluation of the near-surface wind field over the Adriatic region: local wind characteristics in the convection-permitting model ensemble. *Climate Dynamics*, 62(6), 4617–4634. <https://doi.org/10.1007/S00382-023-06703-Z/METRICS>
- Best, M. J., Pryor, M., Clark, D. B., Rooney, G. G., Essery, R. . L. H., Ménard, C. B., Edwards, J. M., Hendry, M. A., Porson, A., Gedney, N., Mercado, L. M., Sitch, S., Blyth, E., Boucher, O., Cox, P. M., Grimmond, C. S. B., & Harding, R. J. (2011). The Joint UK Land Environment Simulator (JULES), model description – Part 1: Energy and water fluxes. *Geoscientific Model Development*, 4(3), 677–699. <https://doi.org/10.5194/gmd-4-677-2011>
- Bohnenstengel, S. I., Evans, S., Clark, P. A., & Belcher, S. E. (2011). Simulations of the London urban heat island. *Quarterly Journal of the Royal Meteorological Society*, 137(659), 1625–1640. <https://doi.org/10.1002/qj.855>
- Boutle, I. A., Eyre, J. E. J., & Lock, A. P. (2014). Seamless Stratocumulus Simulation across the Turbulent Gray Zone. *Monthly Weather Review*, 142(4), 1655–1668. <https://doi.org/10.1175/MWR-D-13-00229.1>
- Brown, A., Dowdy, A., & Lane, T. P. (2024). Convection-permitting climate model representation of severe convective wind gusts and future changes in southeastern Australia. *Natural Hazards and Earth System Sciences*, 24(9), 3225–3243. <https://doi.org/10.5194/NHESS-24-3225-2024>
- Bryan, G. H., Wyngaard, J. C., & Fritsch, J. M. (2003). Resolution requirements for the simulation of deep moist convection. *Monthly Weather Review*, 131(10), 2394–2416. [https://doi.org/10.1175/1520-0493\(2003\)131<2394:RRFTSO>2.0.CO;2](https://doi.org/10.1175/1520-0493(2003)131<2394:RRFTSO>2.0.CO;2)
- Buonomo, E., Savage, N., Dong, G., Becker, B., Jones, R. G., Tian, Z., & Sun, L. (2024). Tropical Cyclone Changes in Convection-Permitting Regional Climate Projections: A Study Over the Shanghai Region. *Journal of Geophysical Research: Atmospheres*, 129(5), e2023JD038508. <https://doi.org/10.1029/2023JD038508;WGROU:STRING:PUBLICATION>
- Bush, M., Allen, T., Bain, C., Boutle, I., Edwards, J., Finnenkoetter, A., Franklin, C., Hanley, K., Lean, H., Lock, A., Manners, J., Mittermaier, M., Morcrette, C., North, R., Petch, J., Short, C., Vosper, S., Walters, D., Webster, S., ... Zerroukat, M. (2020). The first Met Office Unified Model-JULES Regional Atmosphere and Land configuration, RAL1. *Geoscientific Model Development*, 13(4), 1999–2029.

<https://doi.org/10.5194/gmd-13-1999-2020>

- Charney, J. G., & Phillips, N. A. (1953). NUMERICAL INTEGRATION OF THE QUASI-GEOSTROPHIC EQUATIONS FOR BAROTROPIC AND SIMPLE BAROCLINIC FLOWS. *Journal of Meteorology*, 10(2), 71–99. [https://doi.org/10.1175/1520-0469\(1953\)010<0071:niotqg>2.0.co;2](https://doi.org/10.1175/1520-0469(1953)010<0071:niotqg>2.0.co;2)
- Clark, P., Roberts, N., Lean, H., Ballard, S. P., & Charlton-Perez, C. (2016). Convection-permitting models: A step-change in rainfall forecasting. In *Meteorological Applications* (Vol. 23, Issue 2, pp. 165–181). John Wiley and Sons Ltd. <https://doi.org/10.1002/met.1538>
- Cortés-Hernández, V. E., Caillaud, C., Bellon, G., Brisson, E., Alias, A., & Lucas-Picher, P. (2024). Evaluation of the convection permitting regional climate model CNRM-AROME on the orographically complex island of Corsica. *Climate Dynamics*, 62(6), 4673–4696. <https://doi.org/10.1007/s00382-024-07232-z>
- Davies, T., Cullen, M. J. P., Malcolm, A. J., Mawson, M. H., Staniforth, A., White, A. A., & Wood, N. (2005). A new dynamical core for the Met Office’s global and regional modelling of the atmosphere. *Quarterly Journal of the Royal Meteorological Society*, 131(608), 1759–1782. <https://doi.org/10.1256/QJ.04.101>
- Di Virgilio, G., Evans, J. P., Ji, F., Tam, E., Kala, J., Andrys, J., Thomas, C., Choudhury, D., Rocha, C., White, S., Li, Y., El Rafei, M., Goyal, R., Riley, M. L., & Lingala, J. (2024). Design, evaluation and future projections of the NARCIIM2.0 CORDEX-CMIP6 Australasia regional climate ensemble. *Geosci. Model Dev. Discuss.. [Preprint]*, 28(5), 1251–1285. <https://doi.org/10.5194/HESS-28-1251-2024>
- Donat, M. G., Lowry, A. L., Alexander, L. V., O’gorman, P. A., & Maher, N. (2017). Addendum: More extreme precipitation in the world’s dry and wet regions. *Nature Climate Change*, 7(2), 154–158. <https://doi.org/10.1038/NCLIMATE3160>
- Donohue, R. (2023). *Australian C4 grass cover percentage. v1*. CSIRO.
- Dowdy, A., Brown, A., Pepler, A., Thatcher, M., Rafter, T., Evans, J., Ye, H., Su, C.-H., Bell, S., & Stassen, C. (2021). Extreme temperature, wind and bushfire weather projections using a standardised method. In *Bureau Research Report – BRR055*. <http://www.bom.gov.au/research/publications/researchreports/BRR-055.pdf>
- Edwards, J. M., & Slingo, A. (1996). Studies with a flexible new radiation code. I: Choosing a configuration for a large-scale model. *Quarterly Journal of the Royal Meteorological Society*, 122(531), 689–719. <https://doi.org/10.1002/QJ.49712253107>
- Fiddes, S. L., Woodhouse, M. T., Utembe, S., Schofield, R., Alexander, S. P., Alroe, J., Chambers, S. D., Chen, Z., Cravigan, L., Dunne, E., Humphries, R. S., Johnson, G., Keywood, M. D., Lane, T. P., Miljevic, B., Omori, Y., Protat, A., Ristovski, Z., Selleck, P., ... Williams, A. G. (2022). The contribution of coral-reef-derived dimethyl sulfide to aerosol burden over the Great Barrier Reef: A modelling study. *Atmospheric Chemistry and Physics*, 22(4), 2419–2445. <https://doi.org/10.5194/acp-22-2419-2022>
- Field, P. R., Hill, A., Shipway, B., Furtado, K., Wilkinson, J., Miltenberger, A., Gordon, H., Grosvenor, D. P., Stevens, R., & Van Weverberg, K. (2023). Implementation of a double moment cloud microphysics scheme in the UK met office regional numerical weather prediction model. *Quarterly Journal of the Royal Meteorological*

- Society*, 149(752), 703–739. <https://doi.org/10.1002/qj.4414>
- Fosser, G., Khodayar, S., & Berg, P. (2015). Benefit of convection permitting climate model simulations in the representation of convective precipitation. *Climate Dynamics*, 44(1–2), 45–60. <https://doi.org/10.1007/S00382-014-2242-1/FIGURES/9>
- Giorgi, F., Jones, C., & Asrar, G. R. (2009). Addressing climate information needs at the regional level: The CORDEX framework. *World Meteorological Organization Bulletin* 58, 175–183.
- Gómez, B., & Miguez-Macho, G. (2017). The impact of wave number selection and spin-up time in spectral nudging. *Quarterly Journal of the Royal Meteorological Society*, 143(705), 1772–1786. <https://doi.org/10.1002/qj.3032>
- Harper, K. L., Lamarche, C., Hartley, A., Peylin, P., Ottlé, C., Bastrikov, V., San Martín, R., Bohnenstengel, S. I., Kirches, G., Boettcher, M., Shevchuk, R., Brockmann, C., & Defourny, P. (2023). A 29-year time series of annual 300m resolution plant-functional-type maps for climate models. *Earth System Science Data*, 15(3), 1465–1499. <https://doi.org/10.5194/essd-15-1465-2023>
- Hartley, A. J., MacBean, N., Georgievski, G., & Bontemps, S. (2017). Uncertainty in plant functional type distributions and its impact on land surface models. *Remote Sensing of Environment*, 203, 71–89. <https://doi.org/10.1016/j.rse.2017.07.037>
- Hastings, D. A., Dunbar, P. K., Elphinstone, G. M., Bootz, M., Murakami, H., Maruyama, H., Masaharu, H., Holland, P., Payne, J., Bryant, N. A., Logan, T. L., Muller, J.-P., Schreier, G., & MacDonald, J. S. (1999). *The Global Land One-kilometer Base Elevation (GLOBE) Digital Elevation Model, Version 1.0*. <http://www.ngdc.noaa.gov/mgg/topo/globe.html>
- Hersbach, H. ., Bell, B., Berrisford, P., Biavati, G., Horányi, A., Sabater, M., J., N., J., Peubey, C., Radu, R., Rozum, I., Schepers, D., Simmons, A., Soci, C., Dee, D., & Thépaut, J.-N. (2018a). *ERA5 hourly data on pressure levels from 1959 to present*. Copernicus Climate Change Service (C3S) Climate Data Store (CDS). <https://doi.org/10.24381/cds.bd0915c6>
- Hersbach, H. ., Bell, B., Berrisford, P., Biavati, G., Horányi, A., Sabater, M., J., N., J., Peubey, C., Radu, R., Rozum, I., Schepers, D., Simmons, A., Soci, C., Dee, D., & Thépaut, J.-N. (2018b). *ERA5 hourly data on single levels from 1959 to present*. Copernicus Climate Change Service (C3S) Climate Data Store (CDS). <https://doi.org/https://doi.org/10.24381/cds.adbb2d47>
- Hersbach, H., Bell, B., Berrisford, P., Hirahara, S., Horányi, A., Muñoz-Sabater, J., Nicolas, J., Peubey, C., Radu, R., Schepers, D., Simmons, A., Soci, C., Abdalla, S., Abellan, X., Balsamo, G., Bechtold, P., Biavati, G., Bidlot, J., Bonavita, M., ... Thépaut, J. N. (2020). The ERA5 global reanalysis. *Quarterly Journal of the Royal Meteorological Society*, 146(730), 1999–2049. <https://doi.org/10.1002/qj.3803>
- Holloway, C. E., Woolnough, S. J., & Lister, G. M. S. (2013). The effects of explicit versus parameterized convection on the MJO in a large-domain high-resolution tropical case study. Part I: Characterization of large-scale organization and propagation. *Journal of the Atmospheric Sciences*, 70(5), 1342–1369. <https://doi.org/10.1175/JAS-D-12-0227.1>
- Howard, E., Su, C. H., Stassen, C., Naha, R., Ye, H., Pepler, A., Bell, S. S., Dowdy, A. J., Tucker, S. O., & Franklin, C. (2024). Performance and process-based

- evaluation of the BARPA-R Australasian regional climate model version 1. *Geoscientific Model Development*, 17(2), 731–757. <https://doi.org/10.5194/GMD-17-731-2024>
- Huang, Z., Zhong, L., Ma, Y., & Fu, Y. (2021). Development and evaluation of spectral nudging strategy for the simulation of summer precipitation over the Tibetan Plateau using WRF (v4.0). *Geoscientific Model Development*, 14(5), 2827–2841. <https://doi.org/10.5194/gmd-14-2827-2021>
- Huffman, G., Bolvin, D., Braithwaite, D., Hsu, K., Joyce, R., & Xie, P. (2018). *Global Precipitation Measurements (GPM) Integrated Multi-satellitE Retrievals (IMERG) L3 Half Hourly 0.1 degree × 0.1 degree v5*.
- Jakob, D., Black, M., Hague, B., Pepler, A., Bengner, N., Bhardwaj, D., Hoffman, D., Rogers, C., Peter, J., Ramsey, H., Udy, D., Gammon, A., Grose, M., & Narsey, S. (2025). *Climate Hazard Information developed for use in Climate Risk Assessment*.
- Jiang, X., Howard, E., Su, C.-H., Isphording, R., Ng, B., Chapman, S., Ji, F., Grose, M., Sytkus, J., Trancoso, R., Thatcher, M., Narsey, S., Di Virgilio, G., & Kala, J. (2025). Towards benchmarking the dynamically downscaled CMIP6 CORDEX-Australasia ensemble over Australia. *Journal of Southern Hemisphere Earth System Science*, in press.
- Jones, D. A., Wang, W., & Fawcett, R. (2009). High-quality spatial climate data-sets for Australia. *Australian Meteorological and Oceanographic Journal*, 58(4), 233–248. <https://doi.org/10.1071/ES09032>
- Kendon, E. J., Fischer, E. M., & Short, C. J. (2023). Variability conceals emerging trend in 100yr projections of UK local hourly rainfall extremes. *Nature Communications*, 14(1), 1–14. <https://doi.org/10.1038/s41467-023-36499-9>
- Knapp, K. R., Kruk, M. C., Levinson, D. H., Diamond, H. J., & Neumann, C. J. (2010). The international best track archive for climate stewardship (IBTrACS). *Bulletin of the American Meteorological Society*, 91(3), 363–376. <https://doi.org/10.1175/2009BAMS2755.1>
- Kruk, M. C., Knapp, K. R., & Levinson, D. H. (2010). A technique for combining global tropical cyclone best track data. *Journal of Atmospheric and Oceanic Technology*, 27(4), 680–692. <https://doi.org/10.1175/2009JTECHA1267.1>
- Langendijk, G. S., Rechid, D., Sieck, K., & Jacob, D. (2021). Added value of convection-permitting simulations for understanding future urban humidity extremes: case studies for Berlin and its surroundings. *Weather and Climate Extremes*, 33, 100367. <https://doi.org/10.1016/j.wace.2021.100367>
- Lean, H. W., Theeuwes, N. E., Baldauf, M., Barkmeijer, J., Bessardon, G., Blunn, L., Bojarova, J., Boutle, I. A., Clark, P. A., Demuzere, M., Dueben, P., Frogner, I. L., de Haan, S., Harrison, D., Heerwaarden, C. van, Honnert, R., Lock, A., Marsigli, C., Masson, V., ... Yang, X. (2024). The hectometric modelling challenge: Gaps in the current state of the art and ways forward towards the implementation of 100-m scale weather and climate models. In *Quarterly Journal of the Royal Meteorological Society* (Vol. 150, Issue 765, pp. 4671–4708). John Wiley and Sons Ltd. <https://doi.org/10.1002/qj.4858>
- Lee, D., Min, S. K., Park, I. H., Ahn, J. B., Cha, D. H., Chang, E. C., & Byun, Y. H. (2022). Enhanced Role of Convection in Future Hourly Rainfall Extremes Over

- 
- South Korea. *Geophysical Research Letters*, 49(22), 71–95.  
<https://doi.org/10.1029/2022GL099727>
- Liu, C., Ikeda, K., Prein, A., Scaff, L., Dominguez, F., Rasmussen, R., Huang, Y., Dudhia, J., Wang, W., Chen, F., Xue, L., Fita, L., Lagos-Zúñiga, M., Lavado-Casimiro, W., Masiokas, M., Puhales, F., & Yepes, L. J. (2025). Convection-permitting climate simulations over South America: Experimentation during different phases of ENSO. *Atmospheric Research*, 316, 107936.  
<https://doi.org/10.1016/j.atmosres.2025.107936>
- Lock, A. P., Brown, A. R., Bush, M. R., Martin, G. M., & Smith, R. N. B. (2000). A New Boundary Layer Mixing Scheme. Part I: Scheme Description and Single-Column Model Tests. *Monthly Weather Review*, 128(9), 3187–3199.  
[https://doi.org/10.1175/1520-0493\(2000\)128<3187:ANBLMS>2.0.CO;2](https://doi.org/10.1175/1520-0493(2000)128<3187:ANBLMS>2.0.CO;2)
- Lucas-Picher, P., Argüeso, D., Brisson, E., Tramblay, Y., Berg, P., Lemonsu, A., Kotlarski, S., & Caillaud, C. (2021). Convection-permitting modeling with regional climate models: Latest developments and next steps. In *Wiley Interdisciplinary Reviews: Climate Change* (Vol. 12, Issue 6, p. e731). John Wiley & Sons, Ltd.  
<https://doi.org/10.1002/wcc.731>
- Luu, L. N., Vautard, R., Yiou, P., & Soubeyroux, J. M. (2022). Evaluation of convection-permitting extreme precipitation simulations for the south of France. *Earth System Dynamics*, 13(1), 687–702. <https://doi.org/10.5194/esd-13-687-2022>
- Mann, G. W., Carslaw, K. S., Spracklen, D. V., Ridley, D. A., Manktelow, P. T., Chipperfield, M. P., Pickering, S. J., & Johnson, C. E. (2010). Description and evaluation of GLOMAP-mode: A modal global aerosol microphysics model for the UKCA composition-climate model. *Geoscientific Model Development*, 3(2), 519–551. <https://doi.org/10.5194/gmd-3-519-2010>
- Manners, J., Edwards, J. M., Hill, P., & Thelen, J.-C. (2024). *SOCRATES (Suite Of Community RAdiative Transfer codes based on Edwards and Slingo)*.  
[https://code.metoffice.gov.uk/trac/socrates/attachment/wiki/WikiStart/socrates\\_techguide.pdf](https://code.metoffice.gov.uk/trac/socrates/attachment/wiki/WikiStart/socrates_techguide.pdf)
- Maybee, B., Marsham, J. H., Klein, C. M., Parker, D. J., Barton, E. J., Taylor, C. M., Lewis, H., Sanchez, C., Jones, R. W., & Warner, J. (2024). Wind Shear Effects in Convection-Permitting Models Influence MCS Rainfall and Forcing of Tropical Circulation. *Geophysical Research Letters*, 51(17), e2024GL110119.  
<https://doi.org/10.1029/2024GL110119>
- Meteorology, C. and B. of. (2021). *ESCI Project Final Report (Electricity Sector Climate Information (ESCI) Project)*.  
[https://climatechangeinaustralia.gov.au/media/ccia/2.2/cms\\_page\\_media/799/ESCI Project final report\\_210721.pdf](https://climatechangeinaustralia.gov.au/media/ccia/2.2/cms_page_media/799/ESCI Project final report_210721.pdf)
- Poncet, N., Lucas-Picher, P., Tramblay, Y., Thirel, G., Vergara, H., Gourley, J., & Alias, A. (2024). Does a convection-permitting regional climate model bring new perspectives on the projection of Mediterranean floods? *Natural Hazards and Earth System Sciences*, 24(4), 1163–1183. <https://doi.org/10.5194/nhess-24-1163-2024>
- Porson, A., Clark, P. A., Harman, I. N., Best, M. J., & Belcher, S. E. (2010). Implementation of a new urban energy budget scheme into MetUM. Part II: Validation against observations and model intercomparison. *Quarterly Journal of*

- 
- the Royal Meteorological Society*, 136(651), 1530–1542.  
<https://doi.org/10.1002/qj.572>
- Potvin, C. K., & Flora, M. L. (2015). Sensitivity of Idealized Supercell Simulations to Horizontal Grid Spacing: Implications for Warn-on-Forecast. *Monthly Weather Review*, 143(8), 2998–3024. <https://doi.org/10.1175/MWR-D-14-00416.1>
- Rennie, S., Franklin, C., Cooper, S., Roux, B., Steinle, P., Zidkheri, M., Eizenberg, N., Warren, R., Krysta, M., Khanarmuei, M., Smith, F., Smith, A., Samrat, N., Griffin, C., & Brook, J. (2025). ACCESS-A: Developing convective scale NWP for the Australian continent. *In Prep*.
- Schroeter, B. J. E., Ng, B., Takbash, A., Rafter, T., & Thatcher, M. (2024). A Comprehensive Evaluation of Mean and Extreme Climate for the Conformal Cubic Atmospheric Model (CCAM). *Journal of Applied Meteorology and Climatology*, 63(9), 997–1018. <https://doi.org/10.1175/JAMC-D-24-0004.1>
- Sekizawa, S., Nakamura, H., & Kosaka, Y. (2023). Interannual Variability of the Australian Summer Monsoon Sustained through Internal Processes: Wind-Evaporation Feedback, Dynamical Air-Sea Interaction, and Soil Moisture Memory. *Journal of Climate*, 36(3), 983–1000. <https://doi.org/10.1175/JCLI-D-22-0116.1>
- Senior, C. A., Marsham, J. H., Berthou, S., Burgin, L. E., Folwell, S. S., Kendon, E. J., Klein, C. M., Jones, R. G., Mittal, N., Rowell, D. P., Tomassini, L., Vischel, T., Becker, B., Birch, C. E., Crook, J., Dougill, A. J., Finney, D. L., Graham, R. J., Hart, N. C. G., ... Willet, M. R. (2021). Convection-permitting regional climate change simulations for understanding future climate and informing decision-making in Africa. *Bulletin of the American Meteorological Society*, 102(6), E1206–E1223. <https://doi.org/10.1175/BAMS-D-20-0020.1>
- Smagorinsky, J. (1963). General Circulation Experiments with the Primitive Equations. *Monthly Weather Review*, 91(3), 99–164. [https://doi.org/10.1175/1520-0493\(1963\)091<0099:gcewtp>2.3.co;2](https://doi.org/10.1175/1520-0493(1963)091<0099:gcewtp>2.3.co;2)
- Stassen, C., Ng, B., Howard, E., Su, C.-H., & Ye, H. (2025). Added value analysis of a CMIP6-based downscaling ensemble for Australian climate projections. *Journal of Southern Hemisphere Earth System Science (in Review)*.
- Stein, T. H. M., Hogan, R. J., Clark, P. A., Halliwell, C. E., Hanley, K. E., Lean, H. W., Nicol, J. C., & Plant, R. S. (2015). The Dymecs project: A Statistical approach for the evaluation of convective storms in high-resolution NWP models. *Bulletin of the American Meteorological Society*, 96(6), 939–951. <https://doi.org/10.1175/BAMS-D-13-00279.1>
- Stevens, B., Fiedler, S., Kinne, S., Peters, K., Rast, S., Müsse, J., Smith, S. J., & Mauritsen, T. (2017). MACv2-SP: A parameterization of anthropogenic aerosol optical properties and an associated Twomey effect for use in CMIP6. *Geoscientific Model Development*, 10(1), 433–452. <https://doi.org/10.5194/gmd-10-433-2017>
- Stratton, R. A., Senior, C. A., Vosper, S. B., Folwell, S. S., Boutle, I. A., Earnshaw, P. D., Kendon, E., Lock, A. P., Malcolm, A., Manners, J., Morcrette, C. J., Short, C., Stirling, A. J., Taylor, C. M., Tucker, S., Webster, S., & Wilkinson, J. M. (2018). A Pan-African Convection-Permitting Regional Climate Simulation with the Met Office Unified Model: CP4-Africa. *Journal of Climate*, 31(9), 3485–3508. <https://doi.org/10.1175/JCLI-D-17-0503.1>

- 
- Su, C.-H., Rennie, S., Dharssi, I., Torrance, J., Smith, A., Le, T., Steinle, P., Stassen, C., Warren, R. A., Wang, C., & Le Marshall, J. (2022). *BARRA2: Development of the next-generation Australian regional atmospheric reanalysis*. <http://www.bom.gov.au/research/publications/researchreports/BRR-067.pdf>
- Su, C.-H., Rennie, S., Torrance, J., Howard, E., Stassen, C., Lipson, M., Warren, R. A., Pepler, A. S., Dharssi, I., & Franklin, C. (2024). *BARRA-C2: Development of the kilometre-scale downscaled atmospheric reanalysis over Australia*.
- Su, C.-H., Stassen, C., Howard, E., Ye, H., Bell, S. S., Pepler, A., Dowdy, A. J., Tucker, S. O., & Franklin, C. (2022). *BARPA: New development of ACCESS-based regional climate modelling for Australian Climate Service*. Bureau Research Report – BRR069. <http://www.bom.gov.au/research/publications/researchreports/BRR-069.pdf>
- Thatcher, M., & McGregor, J. L. (2009). Using a scale-selective filter for dynamical downscaling with the conformal cubic atmospheric model. *Monthly Weather Review*, 137(6), 1742–1752. <https://doi.org/10.1175/2008MWR2599.1>
- Tomassini, L., Willett, M., Sellar, A., Lock, A., Walters, D., Whittall, M., Sanchez, C., Heming, J., Earnshaw, P., Rodriguez, J. M., Ackerley, D., Xavier, P., Franklin, C., & Senior, C. A. (2023). Confronting the Convective Gray Zone in the Global Configuration of the Met Office Unified Model. *Journal of Advances in Modeling Earth Systems*, 15(5), e2022MS003418. <https://doi.org/10.1029/2022MS003418>
- Tucker, S. O., Kendon, E. J., Bellouin, N., Buonomo, E., Johnson, B., & Murphy, J. M. (2022a). Correction to: Evaluation of a new 12 km regional perturbed parameter ensemble over Europe (*Climate Dynamics*, (2022), 58, 3-4, (879-903), 10.1007/s00382-021-05941-3). In *Climate Dynamics* (Vol. 58, Issues 3–4, p. 905). Copernicus GmbH. <https://doi.org/10.1007/s00382-021-05985-5>
- Tucker, S. O., Kendon, E. J., Bellouin, N., Buonomo, E., Johnson, B., & Murphy, J. M. (2022b). Evaluation of a new 12 km regional perturbed parameter ensemble over Europe. *Climate Dynamics*, 58(3–4), 879–903. <https://doi.org/10.1007/S00382-021-05941-3/METRICS>
- Van Weverberg, K., Morcrette, C. J., & Boutle, I. (2021). A Bimodal Diagnostic Cloud Fraction Parameterization. Part II: Evaluation and Resolution Sensitivity. *Monthly Weather Review*, 149(3), 859–878. <https://doi.org/10.1175/MWR-D-20-0230.1>
- Van Weverberg, K., Morcrette, C. J., Boutle, I., Furtado, K., & Field, P. R. (2021). A Bimodal Diagnostic Cloud Fraction Parameterization. Part I: Motivating Analysis and Scheme Description. *Monthly Weather Review*, 149(3), 841–857. <https://doi.org/10.1175/MWR-D-20-0224.1>
- Vergara-Temprado, J., Ban, N., Panosetti, D., Schlemmer, L., & Schär, C. (2020). Climate models permit convection at much coarser resolutions than previously considered. *Journal of Climate*, 33(5), 1915–1933. <https://doi.org/10.1175/JCLI-D-19-0286.1>
- Wasko, C., Westra, S., Nathan, R., Pepler, A., Raupach, T. H., Dowdy, A., Johnson, F., Ho, M., McInnes, K. L., Jakob, D., Evans, J., Villarini, G., & Fowler, H. J. (2024). A systematic review of climate change science relevant to Australian design flood estimation. In *Hydrology and Earth System Sciences* (Vol. 28, Issue 5, pp. 1251–1285). Copernicus Publications. <https://doi.org/10.5194/hess-28-1251-2024>
- Weisman, M. L., Skamarock, W. C., & Klemp, J. B. (1997). The resolution dependence



of explicitly modeled convective systems. *Monthly Weather Review*, 125(4), 527–548. [https://doi.org/10.1175/1520-0493\(1997\)125<0527:TRDOEM>2.0.CO;2](https://doi.org/10.1175/1520-0493(1997)125<0527:TRDOEM>2.0.CO;2)

- Wood, N., Staniforth, A., White, A., Allen, T., Diamantakis, M., Gross, M., Melvin, T., Smith, C., Vosper, S., Zerroukat, M., & Thuburn, J. (2014). An inherently mass-conserving semi-implicit semi-Lagrangian discretization of the deep-atmosphere global non-hydrostatic equations. *Quarterly Journal of the Royal Meteorological Society*, 140(682), 1505–1520. <https://doi.org/10.1002/QJ.2235>;WGROU:STRING:PUBLICATION
- Yang, L., Wang, S., Tang, J., Niu, X., & Fu, C. (2019). Impact of nudging parameters on dynamical downscaling over CORDEX East Asia Phase II domain: The case of summer 2003. *Journal of Applied Meteorology and Climatology*, 58(12), 2755–2771. <https://doi.org/10.1175/JAMC-D-19-0152.1>
- Zanaga, D., Van De Kerchove, R., De Keersmaecker, W., Souverijns, N., Brockmann, C., Quast, R., Wevers, J., Grosu, A., Paccini, A., Vergnaud, S., Cartus, O., Santoro, M., Fritz, S., Georgieva, I., Lesiv, M., Carter, S., Herold, M., Li, L., Tsendbazar, N.-E., ... Arino, O. (2021). ESA WorldCover 10 m 2020 v100 (Versión v100) [Data set]. *Zenodo*. <https://doi.org/10.5281/ZENODO.5571936>